On the impact of GNSS ambiguity resolution geometry, ionosphere, time and biases

Khodabandeh, A.; Teunissen, P. J.G.

DOI
10.1007/s00190-017-1084-0

Publication date
2018

Document Version
Final published version

Published in
Journal of Geodesy

J Geod (2018) 92:637–658
https://doi.org/10.1007/s00190-017-1084-0

ORIGINAL ARTICLE

On the impact of GNSS ambiguity resolution: geometry, ionosphere, time and biases

A. Khodabandeh[1] · **P. J. G. Teunissen**[1,2]

Received: 9 June 2017 / Accepted: 1 November 2017 / Published online: 14 November 2017

Abstract Integer ambiguity resolution (IAR) is the key to fast and precise GNSS positioning and navigation. Next to the positioning parameters, however, there are several other types of GNSS parameters that are of importance for a range of different applications like atmospheric sounding, instrumental calibrations or time transfer. As some of these parameters may still require pseudo-range data for their estimation, their response to IAR may differ significantly. To infer the impact of ambiguity resolution on the parameters, we show how the ambiguity-resolved double-differenced phase data propagate into the GNSS parameter solutions. For that purpose, we introduce a canonical decomposition of the GNSS network model that, through its decoupled and decorrelated nature, provides direct insight into which parameters, or functions thereof, gain from IAR and which do not. Next to this qualitative analysis, we present for the GNSS estimable parameters of geometry, ionosphere, timing and instrumental biases closed-form expressions of their IAR precision gains together with supporting numerical examples.

Keywords Global navigation satellite system (GNSS) · Integer ambiguity resolution (IAR) · Canonical differencing (CD) transformation · UD-SD-DD decomposition · Estimable parameters · Precision gain numbers

✉ A. Khodabandeh
amir.khodabandeh@curtin.edu.au

P. J. G. Teunissen
p.teunissen@curtin.edu.au

[1] GNSS Research Centre, Curtin University of Technology, Perth, Australia

[2] Department of Geoscience and Remote Sensing, Delft University of Technology, Delft, The Netherlands

1 Introduction

Integer ambiguity resolution (IAR) is the process of resolving the ambiguous cycles of the carrier-phase measurements as integers. It has found a widespread usage in various global navigation satellite system (GNSS) applications and is considered to be the key to fast and precise GNSS parameter estimation (Teunissen 1995; Tiberius and de Jonge 1995; Teunissen et al. 1997; Han 1997; Hassibi and Boyd 1998; Xu et al. 2012). The goal of IAR is to fully exploit the high precision of the carrier-phase data. Once the unknown ambiguities are resolved, the carrier-phase data will act as very precise pseudo-range data, thus making fast and precise positioning, navigation and attitude determination possible, see, e.g., Jonkman et al. (2000), Hauschild et al. (2008), Giorgi et al. (2012), Gunther and Henkel (2012), Nadarajah et al. (2013), Li et al. (2014), Banville (2016), Odolinski and Teunissen (2017).

Next to the positioning parameters, however, there exist several other types of GNSS parameters that are of great importance for a range of different applications like atmospheric sounding (Coster et al. 1992; Schaer et al. 1995; Liao and Gao 2001), instrumental calibration (Petit et al. 2000; Zhang et al. 2017) or time transfer (Fliegel et al. 1990; Plumb et al. 2005; Delporte et al. 2007). The estimable parameters such as satellite clocks, satellite phase biases and ionospheric delays serve as essential corrections in the IAR-enabled precise point positioning (PPP-RTK) methods (Ge et al. 2008; Laurichesse et al. 2009; Teunissen et al. 2010; Collins et al. 2010; Geng et al. 2012; Odijk et al. 2015). Estimation of the stated parameters often demands an *undifferenced* (UD) formulation. The UD formulation has the advantage over its single-differenced (SD) and double-differenced (DD) counterparts, as it still contains all estimable GNSS

parameters (Teunissen 1995), i.e., none are a priori eliminated.

In our earlier study (Teunissen and Khodabandeh 2014), we showed that there exist estimable parameters, other-than-DD functions, which *cannot* be determined solely from ambiguity-resolved DD phase data. Thus, even after IAR, such parameters do still require pseudo-range (code) data for their estimation. Such parameters will therefore have an IAR response that may differ significantly from the IAR benefit that positioning and zenith tropospheric delay (ZTD) parameters enjoy. It is therefore the goal of the present contribution to show how the ambiguity-resolved DD phase data propagate into the solutions of such GNSS parameters, thus allowing one to infer the impact of ambiguity fixing on the precision of these parameters.

We base our analysis on the UD carrier-phase and code observation equations of a network of n GNSS receivers tracking m satellites on f frequencies. We develop a canonical decomposition of the multivariate GNSS network model consisting of 4 blocks of *decoupled* and *uncorrelated* observation equations. They are formed from (1) satellite- and receiver-averaged components, (2) satellite-averaged SD components, (3) receiver-averaged SD components, and (4) DD components. With the aid of these four blocks, we present closed-form expressions of the precision gain numbers for the estimable parameters, thereby quantifying the parameter precision improvement due to IAR.

This contribution is organized as follows. In Sect. 2, we briefly review and highlight the underlying differences between the UD and DD formulations. Here, we initiate the idea of decomposing the estimable parameters into their DD and other-than-DD components. In Sect. 3 we develop our canonical decomposition of the multivariate GNSS network model. By applying a specific one-to-one transformation to the observations and parameters, we obtain 4 sets of decoupled and uncorrelated observation equations, one of which is the set of DD observation equations that drives integer ambiguity resolution. Due to its structure, one can directly infer which parameters benefit from IAR and which do not. Following this approach, we first conduct a qualitative analysis of the IAR impact in Sect. 4. In Sect. 5 we then quantify the precision gain of the parameters using the concept of *gain numbers* (Teunissen 1997) for which a *geometric* approach is employed to provide further insights into the links between the linear combinations of UD, SD and DD types. It is geometrically demonstrated how the precision gain of a float solution is reduced when it deviates from the subspace of the DD functions. A summary with concluding remarks is provided in Sect. 6.

2 Undifferenced (UD) versus double-differenced (DD)

2.1 Network observation equations

We base our analysis on a network of GNSS receivers r ($r = 1, \ldots, n$), tracking satellites s ($s = 1, \ldots, m$) on frequencies j ($j = 1, \ldots, f$). The corresponding observation equations read (Teunissen and Kleusberg 1998)

$$\begin{aligned} \Delta\phi^s_{r,j} &= \rho^s_r - \mu_j \iota^s_r + \lambda_j a^s_{r,j} \\ \Delta p^s_{r,j} &= \rho^s_r + \mu_j \iota^s_r + d^s_{r,j} \end{aligned} \tag{1}$$

where $\Delta\phi^s_{r,j}$ and $\Delta p^s_{r,j}$ denote the 'observed minus computed' phase and code observations, respectively. The precise orbital corrections are assumed included in the observed minus computed observations. The non-dispersive parameter $\rho^s_r = g^{sT}_r \Delta x_r + dt_r - dt^s$ contains the position/ZTD increments Δx_r, the receiver clock parameter dt_r and the satellite clock parameter dt^s, with g^s_r containing the receiver-satellite direction vector and/or the tropospheric mapping function. Ambiguities $a^s_{r,j} = z^s_{r,j} + \delta_{r,j} - \delta^s_{,j}$, in units of cycles, are composed of the integer part $z^s_{r,j}$ and the receiver/satellite non-integer parts $\delta_{r,j}$ and $\delta^s_{,j}$, respectively. They manifest themselves through their wavelength λ_j. The (first-order) slant ionospheric delay, as experienced on the first frequency, is denoted by ι^s_r. Thus, we have the scalars $\mu_j = (\lambda^2_j/\lambda^2_1)$ linking the ionospheric delays to the observations. The lumped term $d^s_{r,j} = d_{r,j} - d^s_{,j}$ contains the frequency-dependent code receiver and satellite biases $d_{r,j}$ and $d^s_{,j}$, respectively. Apart from $a^s_{r,j}$, the rest of the quantities are all expressed in units of range.

In the following, we use the term 'float' for the solutions *before* IAR and indicate them by the $\hat{.}$-symbol. The term 'fixed' is used for the solutions *after* IAR and indicated by the $\check{.}$-symbol.

2.2 The DD model and its IAR phase data

To understand the role played by IAR in improving the precision of the GNSS parameters, we first briefly review the impact of having resolved ambiguities in the DD model. Let the between-receiver and between-satellite differences be symbolized by $(.)_{1r} = (.)_r - (.)_1$ and $(.)^{1s} = (.)^s - (.)^1$, respectively. The DD version of (1) is then given as

$$\begin{aligned} \Delta\phi^{1s}_{1r,j} &= \rho^{1s}_{1r} - \mu_j \iota^{1s}_{1r} + \lambda_j a^{1s}_{1r,j} \\ \Delta p^{1s}_{1r,j} &= \rho^{1s}_{1r} + \mu_j \iota^{1s}_{1r} \end{aligned} \tag{2}$$

Table 1 Estimable GNSS network-derived parameters formed by a commonly used $\mathcal{S}$-basis (Odijk et al. 2015)

Positions/ZTDs	$\Delta\tilde{x}_r = \Delta x_r - \{\Delta x_1\};\ \ r = \{1\}, 2, \ldots, n$
Ionospheric delays	$\tilde{\iota}^s_r = \iota^s_r + d_{r,GF} - d^s_{,GF}$
Satellite clocks	$d\tilde{t}^s = (dt^s + d^s_{,IF}) - (dt_1 + d_{1,IF}) - \{g_1^{sT}\Delta x_1\}$
Receiver clocks	$d\tilde{t}_r = dt_{1r} + d_{1r,IF};\ \ r \neq 1$
Sat. phase biases	$\tilde{\delta}^s_{,j} = \delta^s_{,j} + \frac{1}{\lambda_j}(\mu_j[d^s_{,GF} - d_{1,GF}] - [d^s_{,IF} - d_{1,IF}]) - \delta_{1,j} - z^s_{1,j}$
Rec. phase biases	$\tilde{\delta}_{r,j} = \delta_{1r,j} + \frac{1}{\lambda_j}(\mu_j d_{1r,GF} - d_{1r,IF}) + z^1_{1r,j};\ \ r \neq 1$
Sat. code biases	$\tilde{d}^s_{,j} = (d^s_{,j} - [d^s_{,IF} + \mu_j d^s_{,GF}]) - (d_{1,j} - [d_{1,IF} + \mu_j d_{1,GF}]);\ \ j > 2$
Rec. code biases	$\tilde{d}_{r,j} = d_{1r,j} - (d_{1r,IF} + \mu_j d_{1r,GF});\ \ r \neq 1,\ j > 2$
Ambiguities	$\tilde{z}^s_{r,j} = z^s_{1r,j} - z^1_{1r,j};\ \ r \neq 1,\ s \neq 1,$
$\mathcal{S}$-basis parameters	$\{\Delta x_1\},\ dt_1, d_{1,j},\ \delta_{1,j},\ z^s_{1,j},\ z^1_{r,j},\ d_{r\neq1,j=1,2},\ d^s_{,j=1,2}$

The additional parameter Δx_1 (within $\{.\}$) is taken as $\mathcal{S}$-basis for the small-to-regional scale networks, i.e., when $g^s_r \approx g^s_1 (r = 2, \ldots, n)$
$(.)_{,IF} = \frac{1}{\mu_2-\mu_1}[\mu_2(.)_{,1} - \mu_1(.)_{,2}];\quad (.)_{,GF} = \frac{1}{\mu_2-\mu_1}[(.)_{,2} - (.)_{,1}]$

with $(.)^{1s}_{1r} = (.)^s_{1r} - (.)^1_{1r}$ being the DD symbol. Compare (2) with its UD counterpart (1). The clock terms dt_r/dt^s as well as the biases $d_{r,j}/d^s_{,j}$ and $\delta_{r,j}/\delta^s_{,j}$ are eliminated. The non-dispersive parameter ρ^s_r is reduced to the DD-range parameter ρ^{1s}_{1r} as

$$\rho^{1s}_{1r} = g_r^{1sT}\Delta x_{1r} + g_{1r}^{1sT}\Delta x_1, \tag{3}$$

while the ambiguities $a^s_{r,j}$, in their DD form, become integer-valued, i.e., $a^{1s}_{1r,j} = z^{1s}_{1r,j} \in \mathbb{Z}$. The number of DD phase data $\Delta\phi^{1s}_{1r,j}$ in the single-epoch model (2) is the same as the number of DD ambiguities $a^{1s}_{1r,j}$. Thus, the very precise phase data $\Delta\phi^{1s}_{1r,j}$ have to be *fully* reserved for determining $a^{1s}_{1r,j}$, leaving the less precise DD code data $\Delta p^{1s}_{1r,j}$ to drive the precision of the float solutions $\hat{\rho}^{1s}_{1r}$ and $\hat{\iota}^{1s}_{1r}$ (Teunissen 1997). This situation becomes quite different though, once the float ambiguities $\hat{a}^{1s}_{1r,j}$ are successfully mapped to their integers $\check{a}^{1s}_{1r,j}$. In that case one may treat the integer estimated ambiguities $\check{a}^{1s}_{1r,j}$ as known and deterministic, and move them to the left-hand side of (2) thus making the 'ambiguity-resolved' DD phase data $(\Delta\phi^{1s}_{1r,j} - \lambda_j\check{a}^{1s}_{1r,j})$ act *as if* they are very precise code data. The precision of the fixed solutions $\check{\rho}^{1s}_{1r}$ and $\check{\iota}^{1s}_{1r}$ would then be dominated by that of the 'ambiguity-resolved' phase data. In other words, the unknown parameters ρ^{1s}_{1r} and ι^{1s}_{1r} can then be determined *fully* by means of the 'ambiguity-resolved' phase-only model

$$\left(\Delta\phi^{1s}_{1r,j} - \lambda_j\check{a}^{1s}_{1r,j}\right) = \rho^{1s}_{1r} - \mu_j\iota^{1s}_{1r}, \quad j = 1, \ldots, f \tag{4}$$

Thus, in the single-epoch case, the precision of the solutions $\check{\iota}^{1s}_{1r}$ and $\check{\rho}^{1s}_{1r}$ (and therefore $\Delta\check{x}_r$) experiences two orders of magnitude improvement, as the standard-deviation of the phase data is almost 100 times smaller than its code counterpart.

2.3 The UD model and its estimable parameters

We now turn our attention to the UD formulation of (1). In this case, there exist components other than the DD parameters ρ^{1s}_{1r} and ι^{1s}_{1r} which *cannot* be fully determined by the ambiguity-resolved DD phase data. Even after IAR, such components still require code data for their estimation. The question is now whether such components can still benefit from IAR and if so, to what extent.

If we want to work with the UD formulation (1), we first need to eliminate its rank-deficiencies. Due to its rank-deficiency, not all of its parameters are estimable, only combinations of them. A number of parameters, equal to the rank-deficiency, must therefore be chosen as the system's $\mathcal{S}$-basis so as to form a set of minimum constraints that helps recover the system of equations to one of full rank (Baarda 1973; Teunissen 1985). For a commonly used $\mathcal{S}$-basis, a full-rank version of the single-epoch UD model (1) is given as (Odijk et al. 2015)

$$\begin{aligned} \Delta\phi^s_{r,j} &= \tilde{\rho}^s_r - \mu_j\tilde{\iota}^s_r + \lambda_j\tilde{a}^s_{r,j} \\ \Delta p^s_{r,j} &= \tilde{\rho}^s_r + \mu_j\tilde{\iota}^s_r + \tilde{d}^s_{r,j} \end{aligned} \tag{5}$$

with $\tilde{\rho}^s_r = g_r^{sT}\Delta\tilde{x}_r + d\tilde{t}_r - d\tilde{t}^s$, $\tilde{d}^s_{r,j} = \tilde{d}_{r,j} - \tilde{d}^s_{,j}$, and $\tilde{a}^s_{r,j} = \tilde{z}^s_{r,j} + \tilde{\delta}_{r,j} - \tilde{\delta}^s_{,j}$. The estimable parameters are indicated with the $\tilde{.}$-symbol. Their interpretations, together with the choice of $\mathcal{S}$-basis, are given in Table 1. The table shows how each estimable parameter is formed as a certain linear combination of the original parameters. For instance, the estimable receiver clocks $d\tilde{t}_r$ represent the between-receiver SD clocks dt_{1r} that are biased by the 'ionosphere-free' (IF) combination of the receiver code biases, i.e., $d_{1r,IF}$. On the other hand, the estimable slant ionospheric delays $\tilde{\iota}^s_r$ are the true slant ionospheric delays ι^s_r that are biased by the

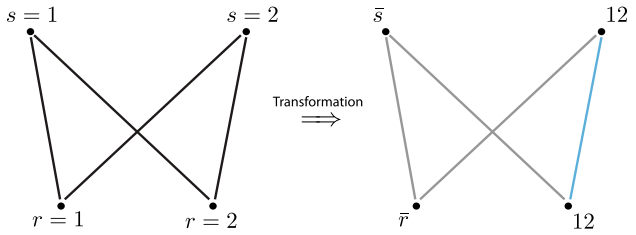

Fig. 1 Visualization of the transformation (6) to receiver pair $r = 1, 2$ tracking satellite pair $s = 1, 2$. After the transformation, the roles of the reference receiver $r = 1$ and satellite $s = 1$ are replaced by those of the 'receiver-average' $\bar{r}$ and the 'satellite-average' $\bar{s}$, respectively

'geometry-free' (GF) combination of the receiver/satellite biases, i.e., $d_{r,GF}/d^s_{,GF}$ (see the table for their definition).

2.4 A UD-SD-DD decomposition

From the DD model (2) we learned that ambiguity-resolved DD phase data are sufficient to estimate the model's DD parameters. As the ambiguity-resolved estimation of these parameters does not need any code data, they can be determined with very high precision. To see how this works out for the estimable parameters of the UD model (5), we introduce a decomposition of the UD model that allows us to bring it into a useful canonical form. This form is created such that it contains the DD formulation (2). As DD components are of a 'differenced' nature, the idea of the decomposition is based on the following two simple facts. Firstly, that any two random variables can be *uniquely* expressed in terms of their *average* and their *difference*. Secondly, that if the two variables are of equal precision and uncorrelated, then also their 'average' and 'difference' are *uncorrelated*.

Consider a receiver pair $r = 1, 2$ tracking the satellite pair $s = 1, 2$. By 'averaging' and 'differencing' both at receiver level and satellite level, the corresponding four-phase observations $\Delta\phi^s_{r,j}$ $(r = 1, 2,\ s = 1, 2)$, on frequency j, undergo the following one-to-one transformation

$$\begin{bmatrix} \Delta\phi^{\bar{s}}_{\bar{r},j} & , & \Delta\phi^{\bar{s}}_{12,j} \\ \Delta\phi^{12}_{\bar{r},j} & , & \Delta\phi^{12}_{12,j} \end{bmatrix} = \begin{bmatrix} \frac{1}{2} & , & \frac{1}{2} \\ -1 & , & 1 \end{bmatrix} \begin{bmatrix} \Delta\phi^1_{1,j} & , & \Delta\phi^1_{2,j} \\ \Delta\phi^2_{1,j} & , & \Delta\phi^2_{2,j} \end{bmatrix} \begin{bmatrix} \frac{1}{2} & , & -1 \\ \frac{1}{2} & , & 1 \end{bmatrix} \tag{6}$$

Accordingly, the role of the reference receiver $r = 1$ is replaced by that of the 'receiver-average' $\bar{r}$. Likewise, the 'satellite-average' $\bar{s}$ replaces the reference satellite $s = 1$ (see Fig. 1). The transformed observations are the satellite- and receiver-averaged component $\Delta\phi^{\bar{s}}_{\bar{r},j}$, the satellite-averaged SD component the $\Delta\phi^{\bar{s}}_{12,j}$, the receiver-averaged SD component $\Delta\phi^{12}_{\bar{r},j}$, and the DD component $\Delta\phi^{12}_{12,j}$. These transformed observations are mutually *uncorrelated* if the four original undifferenced phase observations $\Delta\phi^s_{r,j}$ are uncorrelated and equally precise. To see this, let us present the transformation (6) in its vectorial form as

$$\begin{bmatrix} \Delta\phi^{\bar{s}}_{\bar{r},j} \\ \Delta\phi^{12}_{\bar{r},j} \\ \Delta\phi^{\bar{s}}_{12,j} \\ \Delta\phi^{12}_{12,j} \end{bmatrix} = \begin{bmatrix} \frac{1}{4}, & \frac{1}{4}, & \frac{1}{4}, & \frac{1}{4} \\ -\frac{1}{2}, & \frac{1}{2}, & -\frac{1}{2}, & \frac{1}{2} \\ -\frac{1}{2}, & -\frac{1}{2}, & \frac{1}{2}, & \frac{1}{2} \\ 1, & -1, & -1, & 1 \end{bmatrix} \begin{bmatrix} \Delta\phi^1_{1,j} \\ \Delta\phi^2_{1,j} \\ \Delta\phi^1_{2,j} \\ \Delta\phi^2_{2,j} \end{bmatrix} \tag{7}$$

The zero-correlation property of the transformed observations follows then from the mutually *orthogonal* rows of the above transformation matrix.

By applying the same transformation (6) to the estimable parameters $\tilde{\rho}^s_r, \tilde{\iota}^s_r$ and $\tilde{z}^s_r$ $(r = 1, 2,\ s = 1, 2)$ of the UD model (5), we obtain the following four *decoupled* and *uncorrelated* observation equations

$$\begin{aligned} \Delta\phi^{\bar{s}}_{\bar{r},j} &= \tilde{\rho}^{\bar{s}}_{\bar{r}} - \mu_j \tilde{\iota}^{\bar{s}}_{\bar{r}} + \lambda_j \tilde{a}^{\bar{s}}_{\bar{r},j} \\ \Delta\phi^{12}_{\bar{r},j} &= \tilde{\rho}^{12}_{\bar{r}} - \mu_j \tilde{\iota}^{12}_{\bar{r}} + \lambda_j \tilde{a}^{12}_{\bar{r},j} \\ \Delta\phi^{\bar{s}}_{12,j} &= \tilde{\rho}^{\bar{s}}_{12} - \mu_j \tilde{\iota}^{\bar{s}}_{12} + \lambda_j \tilde{a}^{\bar{s}}_{12,j} \\ \Delta\phi^{12}_{12,j} &= \tilde{\rho}^{12}_{12} - \mu_j \tilde{\iota}^{12}_{12} + \lambda_j \tilde{a}^{12}_{12,j} \end{aligned} \tag{8}$$

A similar set of equations can be obtained for the code data. This set will have the same structure as that of (8), but with the ambiguities absent.

We now show how the decoupled and uncorrelated property of (8) helps us in understanding how GNSS parameters are impacted by integer ambiguity resolution (IAR). First note, since every phase observation equation has its own unknown ambiguity, that in the single-epoch case, the determination of any of the ρ- and ι-parameters relies solely on the code data. That is, the phase data will not contribute to their determination in case the ambiguities are unknown. Now consider the case of successful IAR. After successful IAR, the DD ambiguity $\tilde{a}^{12}_{12,j} \in \mathbb{Z}$ may be assumed known, which can then be moved to the left-hand side of the last equation of (8), thus allowing for a significant improvement in the precision of the float solutions of the DD parameters $\tilde{\rho}^{12}_{12}$ and $\tilde{\iota}^{12}_{12}$, just as it happened in the DD model (4). The remaining parameters of (8), however, do *not* benefit from IAR. They do not benefit, since they themselves are decoupled from the DD equation, while at the same time their equations phase and code data are uncorrelated with the DD data used for IAR. Thus, none of the ρ-, ι- and a-parameters of the first three equations of (8) benefit from IAR.

Since the parameters of (8) can also be used to reconstruct their original undifferenced versions (e.g., $\tilde{\rho}^1_1 = \tilde{\rho}^{\bar{s}}_{\bar{r}} - \frac{1}{2}\tilde{\rho}^{12}_{\bar{r}} - \frac{1}{2}\tilde{\rho}^{\bar{s}}_{12} + \frac{1}{4}\tilde{\rho}^{12}_{12}$), one can infer how the precision improvement due to IAR propagates. Consider, for instance, the between-satellite SD ionospheric parameter $\tilde{\iota}^{12}_1$. Its float and fixed

solutions can be expressed in terms of those of the components $\tilde{\imath}_{\tilde{r}}^{12}$ and $\tilde{\imath}_{12}^{12}$. They, respectively, read

$$\begin{aligned} \text{float}: &\quad \hat{\imath}_1^{12} = -\tfrac{1}{2}\,\hat{\imath}_{12}^{12} + \hat{\imath}_{\tilde{r}}^{12} \\ \text{fixed}: &\quad \check{\imath}_1^{12} = -\tfrac{1}{2}\,\check{\imath}_{12}^{12} + \hat{\imath}_{\tilde{r}}^{12} \end{aligned} \tag{9}$$

While the DD float solution $\hat{\imath}_{12}^{12}$ changes to its fixed version $\check{\imath}_{12}^{12}$ after ambiguity fixing, the float solution $\hat{\imath}_{\tilde{r}}^{12}$ remains *unchanged* as it belongs to the second equation of (8), being uncorrelated with the float ambiguities $\hat{a}_{12,j}^{12}$. In the next section, we generalize the above ideas to the multivariate GNSS network case.

3 Canonical decomposition of the GNSS model

3.1 A multivariate representation

The transformations (6) and (7) are limited in the sense that they apply to equally precise phase data of only a single receiver pair tracking a single satellite pair. To generalize the transformation, we first formulate the GNSS model in multivariate form. We therefore define the phase observation vector of receiver r as $\phi_r^S = [\phi_{r,1}^{S^T}, \ldots, \phi_{r,f}^{S^T}]^T \in \mathbb{R}^{fm}$, $\phi_{r,j}^S = [\Delta\phi_{r,j}^1, \ldots, \Delta\phi_{r,j}^m]^T$, $j = 1, \ldots, f$, with a likewise definition for the code observation vector p_r^S. For the n receivers, the network observation matrices are defined as $\phi_R^S = [\phi_1^S, \ldots, \phi_n^S]$ and $p_R^S = [p_1^S, \ldots, p_n^S]$. The multivariate formulation of the full-rank observation Eq. (5) becomes then

$$\begin{aligned} \phi_R^S &= (e_f \otimes I_m)\,\tilde{\rho}_R^S - (\mu \otimes I_m)\,\tilde{\imath}_R^S + (\Lambda \otimes I_m)\,\tilde{a}_R^S \\ p_R^S &= (e_f \otimes I_m)\,\tilde{\rho}_R^S + (\mu \otimes I_m)\,\tilde{\imath}_R^S + (E \otimes I_m)\,\tilde{d}_R^S \end{aligned} \tag{10}$$

The $m \times n$ matrices $\tilde{\rho}_R^S$ and $\tilde{\imath}_R^S$ contain the estimable parameters $\tilde{\rho}_r^s$ and $\tilde{\imath}_r^s$, respectively. The f-vectors e_f and μ, respectively, contain 'ones' and 'μ_j' ($j = 1, \ldots, f$). The $f \times f$ diagonal matrix Λ contains the wavelengths λ_j, through which the $fm \times n$ ambiguity matrix $\tilde{a}_R^S$ is linked to the phase data ϕ_R^S. According to Table 1, the estimable code biases $\tilde{d}_{r,j}^s = \tilde{d}_{r,j} - \tilde{d}_{,j}^s$ are only present in the third frequency and beyond (i.e., $j > 2$). In contrast to the ambiguity matrix $\tilde{a}_R^S$, the dimension of the code-bias matrix $\tilde{d}_R^S$ is $(f-2)m \times n$. Therefore, the first two columns of the identity matrix I_f are eliminated to form the $f \times (f-2)$ matrix E. The symbol $\otimes$ is the Kronecker matrix product (Henderson et al. 1983).

The stochastic model of the observables is assumed given as

$$\mathsf{D}\begin{bmatrix} \phi_r^S \\ p_r^S \end{bmatrix} = c_r^2 \begin{bmatrix} C_\phi & 0 \\ 0 & C_p \end{bmatrix} \otimes C_S, \quad r = 1, \ldots, n \tag{11}$$

with $\mathsf{D}(.)$ being the dispersion operator. The $m \times m$ cofactor matrix C_S captures the satellite elevation dependency. The scalars c_r^2 ($r = 1, \ldots, n$) are receiver-dependent cofactors, structuring the $n \times n$ diagonal matrix C_R. The $f \times f$ positive-definite matrices C_ϕ and C_p are the cofactor matrices of the phase and code observable types, respectively.

3.2 The canonical differencing (CD) transformation

We now generalize the transformations (6) and (7) to the multivariate case. The idea is again to decompose the phase and code data ϕ_R^S and p_R^S into four *uncorrelated* blocks. The $nfm \times nfm$ multivariate generalization of (7) is given as

$$T_{\text{CD}} = \begin{bmatrix} e_n^+ \\ D_n^T \end{bmatrix} \otimes \begin{bmatrix} I_f \otimes e_m^+ \\ I_f \otimes D_m^T \end{bmatrix} \tag{12}$$

in which the matrices D_m and D_n take care of the differencing and the vectors e_m^+ and e_n^+ of the averaging. The $m \times (m-1)$ matrix D_m forms between-satellite differences, while the $n \times (n-1)$ matrix D_n forms between-receiver differences. Their columns are, respectively, orthogonal to the vectors of ones e_m and e_n, i.e., $D_m^T e_m = 0$ and $D_n^T e_n = 0$. The averaging operators, e_m^+ and e_n^+, are given as the weighted pseudo-inverses,

$$\begin{aligned} \text{Satellite-averaging}: &\quad e_m^+ = \tfrac{1}{e_m^T C_S^{-1} e_m} e_m^T C_S^{-1} \\ \text{Receiver-averaging}: &\quad e_n^+ = \tfrac{1}{e_n^T C_R^{-1} e_n} e_n^T C_R^{-1} \end{aligned} \tag{13}$$

The multivariate transformation (12) will be referred to as the *canonical differencing* (CD) transformation (Fig. 2). It is not difficult to verify that the transformation is one-to-one. The CD-transformation will now allow us to transform the multivariate GNSS model (10) into an easy-to-use canonical form.

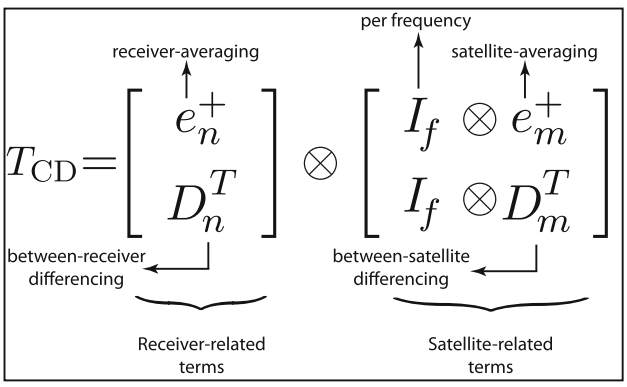

Fig. 2 The CD-transformation: interpretation and functionality of its components

3.3 CD-transformed observations and parameters

We first apply the transformation to the phase and code observations, thus giving $T_{\mathrm{CD}}\mathrm{vec}(\phi_R^S)$ and $T_{\mathrm{CD}}\mathrm{vec}(p_R^S)$. With (12) and an application of the triple-matrix-product vec-property $\mathrm{vec}(ABC) = (C^T \otimes A)\mathrm{vec}(B)$, we obtain for the transformed phase data $T_{\mathrm{CD}}\mathrm{vec}(\phi_R^S)$ in matrix form,

$$\begin{bmatrix} I_f \otimes e_m^+ \\ I_f \otimes D_m^T \end{bmatrix} \phi_R^S \left[e_n^{+T}, D_n\right] = \begin{bmatrix} \phi_{\bar{r}}^{\bar{s}} & , \phi_{1R}^{\bar{s}} \\ \phi_{\bar{r}}^{1S} & , \phi_{1R}^{1S} \end{bmatrix} \Longleftrightarrow$$
$$\phi_R^S = \left[I_f \otimes e_m, I_f \otimes D_m^{+T}\right] \begin{bmatrix} \phi_{\bar{r}}^{\bar{s}} & , \phi_{1R}^{\bar{s}} \\ \phi_{\bar{r}}^{1S} & , \phi_{1R}^{1S} \end{bmatrix} \begin{bmatrix} e_n^T \\ D_n^+ \end{bmatrix} \tag{14}$$

in which we used the notation $(.)^{1S} = D_m^T(.)^S$ and $(.)_{1R} = (.)_R D_n$. The superscript $\bar{s}$ and subscript $\bar{r}$ refer to the 'satellite-' and 'receiver-averaged' components, respectively. Thus, $(.)^{\bar{s}} = e_m^+(.)^S$ and $(.)_{\bar{r}} = (.)_R e_n^{+T}$. The pseudo-inverses of D_m and D_n are defined as $D_m^+ = (D_m^T C_S D_m)^{-1} D_m^T C_S$ and $D_n^+ = (D_n^T C_R D_n)^{-1} D_n^T C_R$, respectively. A similar decomposition as (14) can be obtained for the code data p_R^S.

The decomposition (14) achieves that the undifferenced raw GNSS data ϕ_R^S/p_R^S is decomposed into the following four uncorrelated blocks of data (Fig. 3):

1. Satellite- and receiver-averaged components $\phi_{\bar{r}}^{\bar{s}}/p_{\bar{r}}^{\bar{s}}$,
2. Satellite-averaged SD components $\phi_{1R}^{\bar{s}}/p_{1R}^{\bar{s}}$,
3. Receiver-averaged SD components $\phi_{\bar{r}}^{1S}/p_{\bar{r}}^{1S}$,
4. DD components $\phi_{1R}^{1S}/p_{1R}^{1S}$.

Since the averaging operators e_m^+ and e_n^+ are, respectively, orthogonal to the differencing operators D_m and D_n (i.e., $e_m^+ C_S D_m = 0$ and $e_n^+ C_R D_n = 0$), these four blocks of data are mutually *uncorrelated*.

Just as with the phase and code observations, we also apply the CD-transformation to the estimable parameters of the multivariate GNSS model (10). This will then transform $\tilde{\rho}_R^S$, $\tilde{\imath}_R^S$, $\tilde{a}_R^S$, and $\tilde{d}_R^S$ accordingly. In case of the estimable code biases $\tilde{d}_R^S$, the identity matrix I_f, in (14), must be replaced by its lower-dimension version I_{f-2} and in case of $\tilde{\rho}_R^S$ and $\tilde{\imath}_R^S$, the identity matrix I_f is replaced by '1'. Thus, if we apply the CD-transformation to the non-dispersive matrix $\tilde{\rho}_R^S$, we obtain similar to (14) the decomposition,

$$\begin{bmatrix} e_m^+ \\ D_m^T \end{bmatrix} \tilde{\rho}_R^S \left[e_n^{+T}, D_n\right] = \begin{bmatrix} \tilde{\rho}_{\bar{r}}^{\bar{s}} & , \tilde{\rho}_{1R}^{\bar{s}} \\ \tilde{\rho}_{\bar{r}}^{1S} & , \tilde{\rho}_{1R}^{1S} \end{bmatrix} \Longleftrightarrow$$
$$\tilde{\rho}_R^S = \left[e_m, D_m^{+T}\right] \begin{bmatrix} \tilde{\rho}_{\bar{r}}^{\bar{s}} & , \tilde{\rho}_{1R}^{\bar{s}} \\ \tilde{\rho}_{\bar{r}}^{1S} & , \tilde{\rho}_{1R}^{1S} \end{bmatrix} \begin{bmatrix} e_n^T \\ D_n^+ \end{bmatrix} \tag{15}$$

A similar decomposition is achieved for the other parameters $\tilde{\imath}_R^S$, $\tilde{a}_R^S$, and $\tilde{d}_R^S$ as well.

3.4 The canonical GNSS model

We are now in a position to formulate how the multivariate GNSS model looks like after we have applied the one-to-one CD-transformations to both observations and parameters. It follows that the resulting set of observation equations can then be divided into four uncorrelated and decoupled blocks (Fig. 3):

The *satellite- and receiver-averaged* block:

$$(.)_{\bar{r}}^{\bar{s}} \begin{cases} \phi_{\bar{r}}^{\bar{s}} = e_f\, \tilde{\rho}_{\bar{r}}^{\bar{s}} - \mu\, \tilde{\imath}_{\bar{r}}^{\bar{s}} + \Lambda\, \tilde{a}_{\bar{r}}^{\bar{s}} \\ p_{\bar{r}}^{\bar{s}} = e_f\, \tilde{\rho}_{\bar{r}}^{\bar{s}} + \mu\, \tilde{\imath}_{\bar{r}}^{\bar{s}} + E\, \tilde{d}_{\bar{r}}^{\bar{s}} \end{cases} \tag{16}$$

The *satellite-averaged SD* block:

$$(.)_{1R}^{\bar{s}} \begin{cases} \phi_{1R}^{\bar{s}} = e_f\, \tilde{\rho}_{1R}^{\bar{s}} - \mu\, \tilde{\imath}_{1R}^{\bar{s}} + \Lambda\, \tilde{a}_{1R}^{\bar{s}} \\ p_{1R}^{\bar{s}} = e_f\, \tilde{\rho}_{1R}^{\bar{s}} + \mu\, \tilde{\imath}_{1R}^{\bar{s}} + E\, \tilde{d}_{1R}^{\bar{s}} \end{cases} \tag{17}$$

The *receiver-averaged SD* block:

$$(.)_{\bar{r}}^{1S} \begin{cases} \phi_{\bar{r}}^{1S} = (e_f \otimes I_{m-1})\, \tilde{\rho}_{\bar{r}}^{1S} - (\mu \otimes I_{m-1})\, \tilde{\imath}_{\bar{r}}^{1S} + (\Lambda \otimes I_{m-1})\, \tilde{a}_{\bar{r}}^{1S} \\ p_{\bar{r}}^{1S} = (e_f \otimes I_{m-1})\, \tilde{\rho}_{\bar{r}}^{1S} + (\mu \otimes I_{m-1})\, \tilde{\imath}_{\bar{r}}^{1S} + (E \otimes I_{m-1})\, \tilde{d}_{\bar{r}}^{1S} \end{cases} \tag{18}$$

The *double-differenced (DD)* block:

$$(.)_{1R}^{1S} \begin{cases} \phi_{1R}^{1S} = (e_f \otimes I_{m-1})\, \tilde{\rho}_{1R}^{1S} - (\mu \otimes I_{m-1})\, \tilde{\imath}_{1R}^{1S} + (\Lambda \otimes I_{m-1})\, \tilde{a}_{1R}^{1S} \\ p_{1R}^{1S} = (e_f \otimes I_{m-1})\, \tilde{\rho}_{1R}^{1S} + (\mu \otimes I_{m-1})\, \tilde{\imath}_{1R}^{1S} \end{cases} \tag{19}$$

The four blocks (16–19) represent four sets of *decoupled* and *uncorrelated* observation equations. That is, the four blocks of data are not mutually correlated and each block of observation equations has its own set of parameters, i.e., the four blocks have no parameters in common. Because of these two properties, we can now already get a quick first insight into the impact of IAR. As the DD float ambiguity solution $\hat{\tilde{a}}_{1R}^{1S}$, being a function of only the double-differenced data, is not correlated with the data of the other three blocks, none of the parameters of these three sets of observation equations will benefit from integer ambiguity resolution. That is, they remain *unaffected* by IAR. For instance, the solution of the ionospheric component $\hat{\tilde{\imath}}_{1R}^{\bar{s}}$, being a function of only the satellite-averaged SD components $\phi_{1R}^{\bar{s}}/p_{1R}^{\bar{s}}$, will remain unaffected by IAR (see Fig. 3).

So far we have used the parametrization $\tilde{\rho}_R^S$, both in (15) and in (16–19). These parameters themselves, however, have a further one-to-one parametrization into the position/ZTD

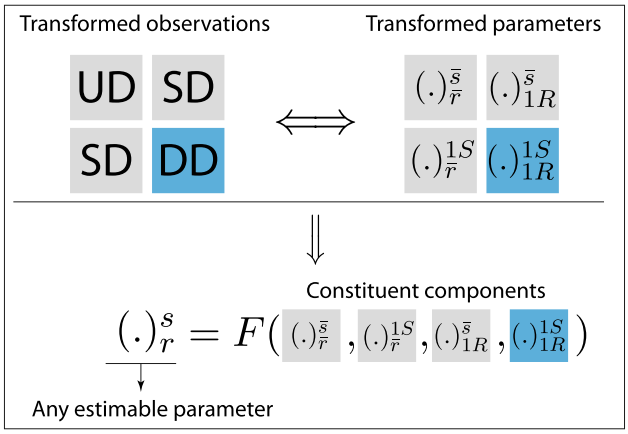

Fig. 3 The four-block decomposition of the GNSS data. Only the estimable functions of the DD block (in blue) are affected by IAR. Any estimable function of the other-than-DD blocks (in gray) remains *unaffected*. Expressing the GNSS estimable parameters in terms of their constituent components, $(.)_r^s = F((.)_{\bar{r}}^{\bar{s}}, (.)_{\bar{r}}^{1S}, (.)_{1R}^{\bar{s}}, (.)_{1R}^{1S})$, shows how they benefit from IAR

increments $\Delta\tilde{x}_R = [\Delta\tilde{x}_1, \ldots, \Delta\tilde{x}_n]$ and the clock parameters $d\tilde{t}^S = [d\tilde{t}^1, \ldots, d\tilde{t}^m]^T$ and $d\tilde{t}_R = [d\tilde{t}_2, \ldots, d\tilde{t}_n]^T$ (cf. 5). To show this, we make use of the multivariate version of $\tilde{\rho}_r^s = g_r^{sT}\Delta\tilde{x}_r + d\tilde{t}_r - d\tilde{t}^s$, being

$$\tilde{\rho}_R^S = \sum_{r=1}^{n}\Big[G_r^S\,\Delta\tilde{x}_R\,u_r u_r^T\Big] + e_m\,d\tilde{t}_R^T\,[0,\,I_{n-1}] - d\tilde{t}^S\,e_n^T \quad (20)$$

with matrices $G_r^S = [g_r^1, \ldots, g_r^m]^T$ $(r = 1, \ldots, n)$ and the n-vectors u_r having zero entries, except their rth entry equal to 1. Substituting (20) into the first expression of (15), the following *one-to-one* correspondence with the ρ-parameters of (16–19) is obtained

$$\begin{aligned}
\tilde{\rho}_{\bar{r}}^{\bar{s}} &= -d\tilde{t}^{\bar{s}} + \sum_{r=1}^{n}\big[G_r^{\bar{s}}\Delta\tilde{x}_R\,u_r u_r^T e_n^{+T}\big] + d\tilde{t}_R^T\,[0,\,I_{n-1}]e_n^{+T}\\
\tilde{\rho}_{1R}^{\bar{s}} &= +d\tilde{t}_R^T + \sum_{r=1}^{n}\big[G_r^{\bar{s}}\,\Delta\tilde{x}_R\,u_r u_r^T D_n\big]\\
\tilde{\rho}_{\bar{r}}^{1S} &= -d\tilde{t}^{1S} + \sum_{r=1}^{n}\big[G_r^{1S}\Delta\tilde{x}_R\,u_r u_r^T e_n^{+T}\big]\\
\tilde{\rho}_{1R}^{1S} &= \quad + \sum_{r=1}^{n}\big[G_r^{1S}\,\Delta\tilde{x}_R\,u_r u_r^T D_n\big]
\end{aligned} \quad (21)$$

This shows, when reading (21) from last to first equation, that the DD component $\tilde{\rho}_{1R}^{1S}$ determines geometry, i.e., the position/ZTD increments $\Delta\tilde{x}_R$ (cf. 3), that the receiver-averaged SD components $\tilde{\rho}_{\bar{r}}^{1S}$ (of size $m-1$) are reserved for the SD satellite clock parameters $d\tilde{t}^{1S}$ (of size $m-1$), while the satellite-averaged SD components $\tilde{\rho}_{1R}^{\bar{s}}$ (of size $n-1$) are reserved for the receiver clock parameters $d\tilde{t}_R$ (of size $n-1$), and finally, that the satellite- and receiver-averaged

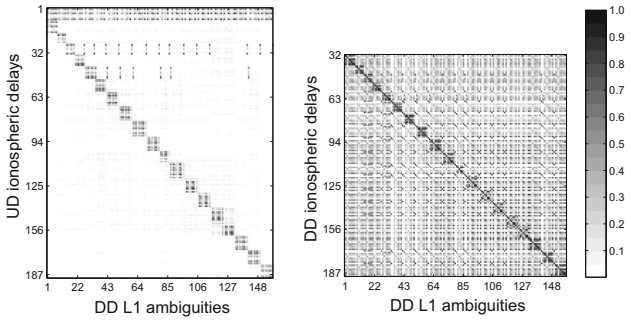

Fig. 4 Absolute values of the cross-correlation matrix between the DD L1 ambiguities (columns) and the estimable ionospheric delays (rows). *Left*: UD estimable ionospheric delays; *right*: DD estimable ionospheric delays. The results are obtained from a network of 20 GPS (L1/L2) stations within Australia

component $\tilde{\rho}_{\bar{r}}^{\bar{s}}$ (a scalar) is reserved for the satellite-averaged clock parameter $d\tilde{t}^{\bar{s}}$.

The above parametrization (21) combined with the uncorrelated and decoupled set of observation equations (16–19) will now be used to further analyze the parameter impact of integer ambiguity resolution.

4 Qualitative analysis of the IAR impact

In this section, we use the canonical decomposition of the multivariate GNSS network model to provide a qualitative insight into the impact of integer ambiguity resolution on the various GNSS parameters.

4.1 Ionospheric parameters $\tilde{\imath}_r^s$

Given the four decoupled and uncorrelated blocks of observation equations (16–19), we are now in a position to address how the ambiguity-resolved phase data propagate into the fixed solutions of any GNSS estimable parameters. In an analogous way to (9), the float and fixed ionospheric solutions can be structured from their constituent components as follows

$$\begin{aligned}
\text{Float}: \quad \hat{\tilde{\imath}}_r^s &= \hat{\tilde{\imath}}_{\bar{r}}^{\bar{s}} + \hat{\tilde{\imath}}_{\bar{r}}^{\bar{s}s} + \hat{\tilde{\imath}}_{\bar{r}r}^{\bar{s}} + \hat{\tilde{\imath}}_{\bar{r}r}^{\bar{s}s}\\
\text{Fixed}: \quad \check{\tilde{\imath}}_r^s &= \check{\tilde{\imath}}_{\bar{r}}^{\bar{s}} + \check{\tilde{\imath}}_{\bar{r}}^{\bar{s}s} + \check{\tilde{\imath}}_{\bar{r}r}^{\bar{s}} + \check{\tilde{\imath}}_{\bar{r}r}^{\bar{s}s}
\end{aligned} \quad (22)$$

The last term $\check{\tilde{\imath}}_{\bar{r}r}^{\bar{s}s} = [\check{\tilde{\imath}}_{1r}^{1s} - \check{\tilde{\imath}}_{1\bar{r}}^{1s}] - [\check{\tilde{\imath}}_{1r}^{1\bar{s}} - \check{\tilde{\imath}}_{1\bar{r}}^{1\bar{s}}]$ is a function of the DD constituent component $\tilde{\imath}_{1R}^{1S}$, driven by the ambiguity-resolved DD phase data (cf. 4), thereby experiencing two orders of magnitude precision improvement. The other three terms, however, are all functions of the other-than-DD constituent components, thus being *uncorrelated* with the float DD ambiguities. These components are driven by the code data. Therefore, they prohibit the precision gain

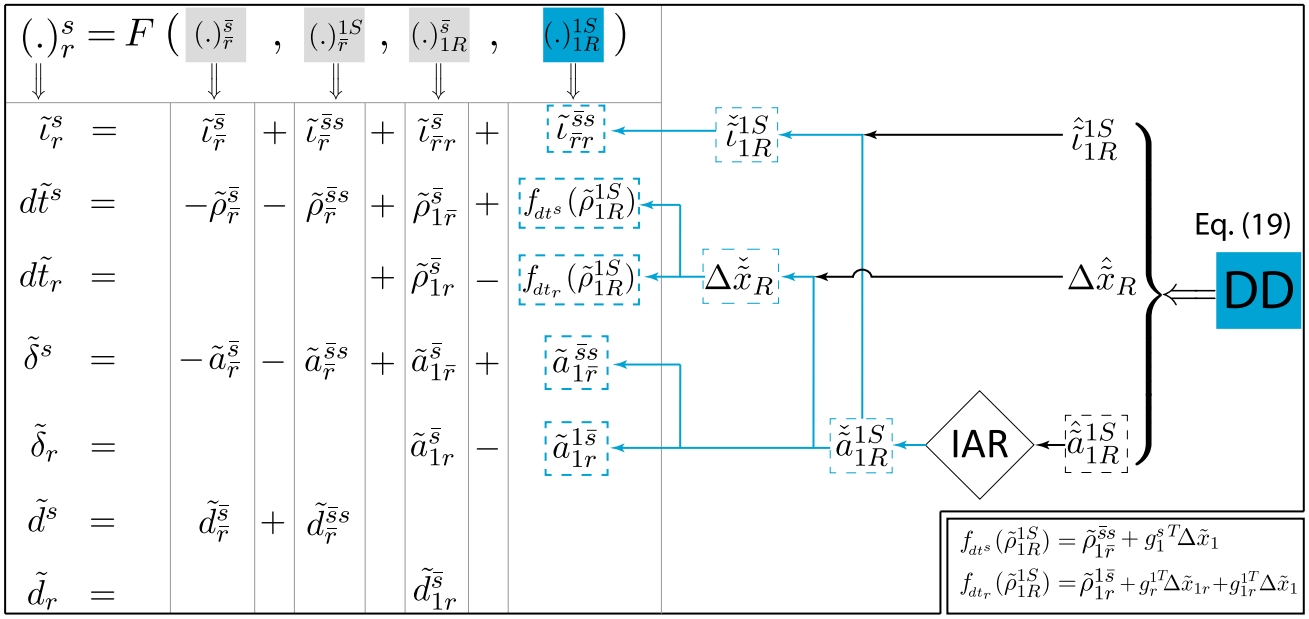

Fig. 5 Diagram showing how the ambiguity-resolved DD phase data, by fixing the DD ambiguities $\tilde{a}^{1S}_{1R}$, propagate into the constituent components and therefore into the estimable parameters (blue lines). As the estimable code biases $\tilde{d}_{r,j}$ and $\tilde{d}^s_{,j}$ do not depend on the DD constituent components $(.)^{1S}_{1R}$, they are uncorrelated with the float ambiguities $\hat{\tilde{a}}^{1S}_{1R}$, thereby remaining unaffected after IAR

of the fixed solution $\check{\tilde{\iota}}^s_r$ to reach the two orders of magnitude level. The presence of these components decreases the correlation between the float solution $\hat{\tilde{\iota}}^s_r$ and the DD float ambiguities. Figure 4 shows absolute values of the cross-correlation matrix between the DD L1 ambiguities (columns) and the estimable ionospheric delays (rows). The results are obtained from a network of 20 GPS stations within Australia. The larger the correlation coefficients, the darker the elements become. In case of the DD ionospheric solutions $\hat{\tilde{\iota}}^{1s}_{1r}$, the correlation coefficients are all significant (right-panel of the figure). This is, however, not the case with the UD ionospheric solutions $\hat{\tilde{\iota}}^s_r$ (left-panel of the figure). In this case, only the ionospheric solutions corresponding to the pivot satellites (diagonal strips) and pivot receivers (the first rows) are correlated with the float DD ambiguities. By 'pivot', we mean those receivers and satellites which their ambiguities are taken as reference to form the DD network ambiguities, see, e.g., de Jonge (1998). The rest of the solutions represent very small correlation coefficients, showing that the presence of UD and SD ionospheric components does indeed decrease the correlation between the float ionospheric delays and the DD ambiguities.

Similar to expression (22), the other estimable parameters given in Table 1 can also be expressed in terms of their constituent components, i.e., the parameters of (16–19). Such expressions are presented in Fig. 5. They are accompanied by a diagram showing how the ambiguity-resolved DD phase data, through fixing the DD ambiguities $\tilde{a}^{1S}_{1R}$, propagate into the constituent components and therefore into the estimable parameters (blue lines).

According to the diagram, the DD observation equations deliver the float DD solutions $\hat{\tilde{\iota}}^{1s}_{1r}$, $\Delta\hat{\tilde{x}}_r$ and $\hat{\tilde{a}}^{1s}_{1r}$. Once IAR is carried out, the ambiguity-resolved DD phase data would then propagate into $\tilde{\iota}^s_r$ *only* through the fixed DD solutions $\check{\tilde{\iota}}^{1s}_{1r}$. As a consequence, when the DD parameters $\tilde{\iota}^{1s}_{1r}$ are a priori known, the float solutions of $\tilde{\iota}^s_r$ become *uncorrelated* with the float ambiguities and therefore *no* precision improvement is obtained by IAR. Practical examples of such are the short inter-station distance scenarios where the between-receiver SD ionospheric delays are assumed to be absent, i.e., $\iota^s_r = \iota^s_1$ $(r = 2, \ldots, n)$. This yields $\tilde{\iota}^s_r = \tilde{\iota}^s_1 + d^s_{r,GF}$ (cf. Table 1), thus $\tilde{\iota}^{1s}_{1r} = 0$. The $(m-1)\times(n-1)$ constraints $\tilde{\iota}^{1s}_{1r} = 0$ reduce the $m \times n$ parameters $\tilde{\iota}^s_r$ to m parameters $\tilde{\iota}^s_1$, but then introducing $(n-1)$ additional estimable parameters $\tilde{d}_{r,GF} = \tilde{\iota}^s_{1r}$ $(r = 2, \ldots, n)$. These parameters are the (scaled) SD receiver 'differential code biases' (DCBs), see, e.g., Schaer (1999) or Zhang and Teunissen (2015). The corresponding decomposition of $\tilde{\iota}^s_1$ and $\tilde{d}_{r,GF}$ is then given as (compare with 22)

$$\begin{aligned} \tilde{\iota}^s_1 &= \tilde{\iota}^{\bar{s}}_{\bar{r}} + \tilde{\iota}^{\bar{s}s}_{\bar{r}} + \tilde{\iota}^{\bar{s}}_{\bar{r}1} + 0 \\ \tilde{d}_{r,GF} &= 0 + 0 + \tilde{\iota}^{\bar{s}}_{1r} + 0 \end{aligned} \tag{23}$$

Thus, neither the ionospheric parameters $\tilde{\iota}^s_1$ nor the receiver DCBs $\tilde{d}_{r,GF}$ benefit from IAR, when the between-receiver SD ionospheric delays are absent.

4.2 Clock parameters $d\tilde{t}_r$ and $d\tilde{t}^s$

Let us now focus on the estimable clock parameters. According to Fig. 5, the ambiguity-resolved DD phase data propagate into $d\tilde{t}_r$ and $d\tilde{t}^s$ *only* through the DD-range solutions $\Delta\check{\tilde{\rho}}^{1s}_{1r}$ and therefore, through the position/ZTD solutions $\Delta\check{\tilde{x}}_R$. Consider the case where $\Delta\tilde{x}_R$ are a priori known. This corresponds to the 'geometry-fixed' scenario when the position of the receivers is assumed to be known, while the ZTDs are a priori corrected. Under these conditions, the DD-range parameters $\Delta\tilde{\rho}^{1s}_{1r}$ are absent, that is, the float solutions of the estimable clocks $d\tilde{t}_r$ and $d\tilde{t}^s$ have *no* dependency on the DD block $(.)^{1S}_{1R}$. Thus, the clock solutions $d\tilde{t}_r$ and $d\tilde{t}^s$ become *uncorrelated* with the float ambiguities and do not benefit from IAR. To what extent these parameters can gain precision improvement does then very much depend on the fixed solution $\Delta\check{\tilde{x}}_R$ and therefore on the DD-range parameter $\tilde{\rho}^{1S}_{1R}$. We come back to this when we quantify the clocks' precision gain as a function of the DD-range's dependency in Sect. 5.

4.3 Phase biases $\tilde{\delta}_{r,j}$ and $\tilde{\delta}^s_{,j}$

In case of the estimable phase biases, the ambiguity-resolved DD phase data propagate to them directly through the DD ambiguities $\tilde{a}^{1S}_{1R}$. Their correlation with the DD ambiguities becomes absent only when the DD ambiguities are a priori known. As no a priori information on the DD ambiguities are often available, these types of parameters would therefore be correlated with the float ambiguities $\tilde{\hat{a}}^{1S}_{1R}$. Figure 6 shows scatter-plots (green dots) of the satellite phase-bias residuals versus those of the DD ambiguities. The residuals are obtained from the difference between the single-epoch and the final filtered solutions. In case of the UD phase biases (top-panel of the figure), the stated correlation is estimated as 0.26. In case of the SD phase biases, however, the correlation increases to 0.61 (bottom-panel of the figure). The reason behind this behavior follows by expressing the estimable phase biases in terms of their constituent components. According to the diagram of Fig. 5, the UD and SD satellite phase biases can be, respectively, expressed as

$$\begin{aligned}\tilde{\delta}^s_{,j} &= -\tilde{a}^{\bar{s}}_{\bar{r}.j} - \tilde{a}^{\bar{s}s}_{\bar{r},j} + \tilde{a}^{\bar{s}}_{1\bar{r},j} + \tilde{a}^{\bar{s}s}_{1\bar{r},j}\\ \tilde{\delta}^{1s}_{,j} &= 0 - \tilde{a}^{1s}_{\bar{r},j} + 0 + \tilde{a}^{1s}_{1\bar{r},j}\end{aligned} \tag{24}$$

The expression (24) reveals that the terms $\tilde{a}^{\bar{s}}_{\bar{r}}$ and $\tilde{a}^{\bar{s}}_{1\bar{r}}$ are eliminated by forming between-satellite differences. Both are uncorrelated with the float ambiguities; thus, their absence in the SD phase biases $\tilde{\delta}^{1s}_{,j}$ increases the stated correlation. To show the dependency of the phase biases on the ambiguities, we also plot the expected phase-bias values when the corresponding L1 ambiguity is given (gray straight lines of Fig. 6). These values show how much the fixed phase-bias solution deviates from its float version (the blue line arrows on the vertical axis), when the difference between the float and fixed ambiguities is given (the blue line arrows on the horizontal axis). The SD phase biases are shown to deviate much more than their UD versions for a given difference between the float and fixed ambiguities, i.e., the SD phase biases benefit more than their UD counterparts.

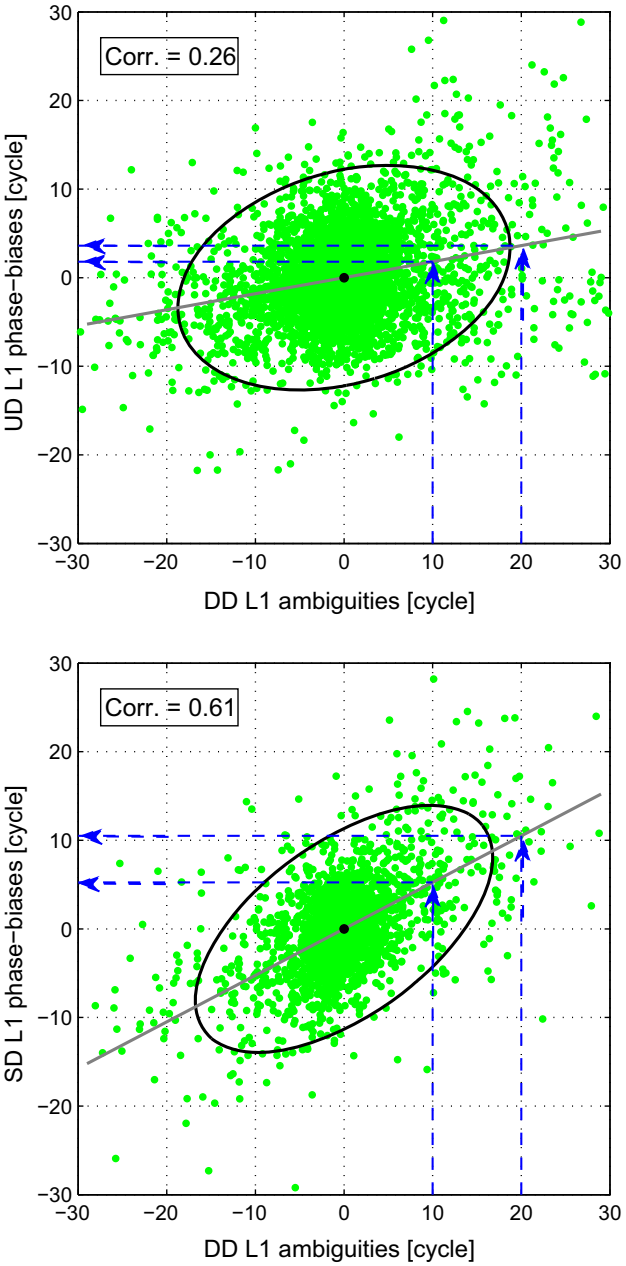

Fig. 6 Scatter-plots (green dots) of the L1 satellite phase-bias residuals (vertical axis) versus that of the DD L1 ambiguities (horizontal axis), together with their 95% confidence ellipses (in black).*Top*: UD satellite phase biases; *bottom*: SD satellite phase biases. The gray straight lines represent expected phase-bias values when the corresponding L1 ambiguity is given. The results are obtained from a network of 20 GPS (L1/L2) stations within Australia

4.4 Code biases $\tilde{d}_{r,j}$ and $\tilde{d}^s_{,j}$

As shown in Fig. 5, the estimable code biases $\tilde{d}_{r,j}$ and $\tilde{d}^s_{,j}$ do not depend on the DD constituent components. They are therefore *uncorrelated* with the float ambiguities $\hat{\tilde{a}}^{1S}_{1R}$, thereby remaining unaffected after IAR. Would one be interested to determine such estimable parameters, no additional IAR step is then required.

5 Precision gain of the GNSS parameters

In the previous section, it was shown how the four-block decomposition (14) facilitates our qualitative analysis of the IAR impact on the GNSS parameters. The analysis was, however, confined to a *single* observational epoch. We now take this one step further and quantify the IAR impact in a *multi-epoch* sense. Since the goal is to study the role played by the integer ambiguities, we consider a multi-epoch scenario where only the integer-valued parameters $z^s_{r,j}$, given in (1), are assumed to be constant in time. For the sake of presentation, from now on we assume the network to be such that the receivers view satellite s from almost the same direction angle, i.e., $g^s_r = g^s_1$ $(r = 1, \ldots, n)$. Thus, $\Delta\tilde{x}_1 = 0$ (cf. Table 1).

5.1 Gain numbers and reduction factors

We use the concept of *gain numbers* (Teunissen 1997) to measure the gain in the parameters' precision due to ambiguity fixing. Let the estimable parameters, in Table 1, be symbolized by the unknown vector x. Any linear function of x can be expressed as $l^T x$ with vector l of the same size of x. Its float and fixed solutions, respectively, read $l^T\hat{x}$ and $l^T\check{x}$. Applying the error propagation law, their variances are given by $l^T Q_{\hat{x}\hat{x}} l$ and $l^T Q_{\check{x}\check{x}} l$, where $Q_{\hat{x}\hat{x}}$ and $Q_{\check{x}\check{x}}$ denote the variance matrices of the float and fixed solutions $\hat{x}$ and $\check{x}$, respectively. The gain number of the float solution $l^T\hat{x}$ is then defined as the variance ratio

$$\gamma(l) = \frac{l^T Q_{\hat{x}\hat{x}} l}{l^T Q_{\check{x}\check{x}} l} = 1 + \frac{l^T (Q_{\hat{x}\hat{x}} - Q_{\check{x}\check{x}}) l}{l^T Q_{\check{x}\check{x}} l} \tag{25}$$

The gain number γ tells us how many times the variance of $l^T\hat{x}$ gets smaller by IAR. Thus, the corresponding standard deviation decreases by a factor of $\sqrt{\gamma}$ (the 'square-root' gain number) after ambiguity fixing. Note that the gain numbers are never smaller than 1 (i.e., $\gamma \geq 1$), as successful ambiguity fixing does not degrade the parameters' precision (Teunissen 1997).

Example To provide further insight into the concept of gain number, float and fixed slant ionospheric solutions of a GPS network have been analyzed. The goal is to *empirically* evaluate the gain number (25). To that end, 120 ionospheric outcomes at every epoch (30 seconds) serve as samples to compute the sample variance

$$l^T Q_{(\hat{x}-\check{x})(\hat{x}-\check{x})} l \approx \frac{1}{h}\sum_{i=1}^{h} [l^T(\hat{x}_i - \check{x}_i)]^2, \tag{26}$$

in which $\hat{x}_i$ and $\check{x}_i$, respectively, denote the float and fixed samples, with h being the number of samples. With (25) and (26), the empirical gain number reads

$$\gamma(l) \approx 1 + \frac{1}{h}\sum_{i=1}^{h} \frac{[l^T(\hat{x}_i - \check{x}_i)]^2}{l^T Q_{\check{x}\check{x}} l} \tag{27}$$

as $Q_{(\hat{x}-\check{x})(\hat{x}-\check{x})} = Q_{\hat{x}\hat{x}} - Q_{\check{x}\check{x}}$. Time series of such empirical gain numbers are presented in Fig. 7. As partial ambiguity resolution, based on subset selection strategy with minimum success rate 99.9%, is applied (Teunissen et al. 1999), a subset of float ambiguities are fixed only after 10 minutes of the network processing. As shown in the figure, empirical gain number of the DD components (blue circles) represents large values and increases over time, reaching its maximum after 37 minutes. This is because of the fact that more ambiguities can be fixed as observations of further epochs are collected. After 37 minutes the full set of ambiguities were already fixed, while the float ionospheric solutions improve in precision over time. That is why their gain numbers start decreasing at that time. Figure 7 also shows empirical gain numbers of the satellite averages (gray crosses). They are close to 1, since they do not benefit from IAR by much. As the averages are obtained by arithmetic averaging and not by that of (13), the corresponding gain numbers are not exactly equal to 1. □

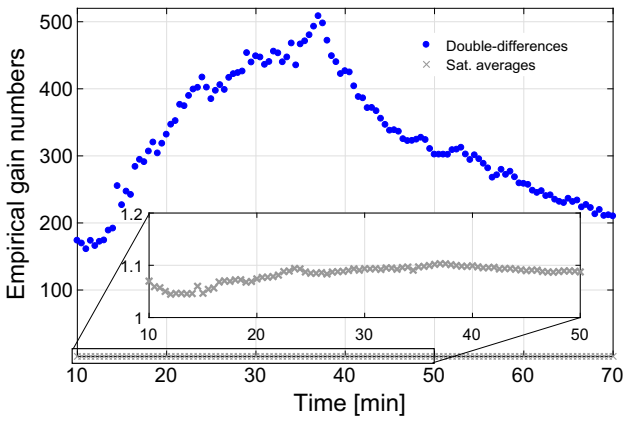

Fig. 7 Empirical gain numbers of the slant ionospheric solutions (DD in blue and satellite averages in gray), given in (27), as a function of time. The results are obtained from a network of 20 GPS (L1/L2) stations within Australia

According to the decompositions (14) and (15), the function $l^T x$ can be decomposed into two constituent components, say, 1) $x_{\mathcal{A}} = l_{\mathcal{A}}^T x$ which benefits from IAR, and 2) $x_{\mathcal{B}} = l_{\mathcal{A}^\perp}^T x$ which is unaffected by IAR. Thus,

$$l^T x = x_{\mathcal{A}} + x_{\mathcal{B}}, \quad \text{or} \quad l = l_{\mathcal{A}} + l_{\mathcal{A}^\perp} \tag{28}$$

As the float solutions $\hat{x}_{\mathcal{A}}$ and $\hat{x}_{\mathcal{B}}$ are *uncorrelated*, we have $\sigma_{\hat{x}_{\mathcal{A}},\hat{x}_{\mathcal{B}}} = l_{\mathcal{A}}^T Q_{\hat{x}\hat{x}} l_{\mathcal{A}^\perp} = 0$. Thus, the vectors $l_{\mathcal{A}}$ and $l_{\mathcal{A}^\perp}$ are *orthogonal* in the metric of $Q_{\hat{x}\hat{x}}$. This explains the orthogonality-symbol '$\perp$' for the subspace $\mathcal{B} = \mathcal{A}^\perp$ representing all linear functions of x that are unaffected by IAR. The complementary subspace $\mathcal{A}$ would therefore represent those linear functions of x that are affected by IAR. For instance, in case of the ionospheric parameters (i.e., $x \mapsto \tilde{\imath}_r^s$), $\mathcal{A}$ represents all the DD functions of $\tilde{\imath}_r^s$. In case of the satellite clocks (i.e., $x \mapsto d\tilde{t}^s$), however, the role of $\mathcal{A}$ is taken by the between-satellite SD functions of $d\tilde{t}^s$ (cf. Fig. 5).

As $\hat{x}_{\mathcal{B}}$ remains unchanged after IAR, i.e., $\check{x}_{\mathcal{B}} = \hat{x}_{\mathcal{B}}$, we have $\sigma_{\check{x}_{\mathcal{A}},\check{x}_{\mathcal{B}}} = \sigma_{\check{x}_{\mathcal{A}},\hat{x}_{\mathcal{B}}}$. But the fixed solution $\check{x}_{\mathcal{A}}$ is a function of $\hat{x}_{\mathcal{A}}$ and the DD float ambiguities, both being uncorrelated with $\check{x}_{\mathcal{B}} = \hat{x}_{\mathcal{B}}$. This means $\sigma_{\check{x}_{\mathcal{A}},\check{x}_{\mathcal{B}}} = 0$ or $l_{\mathcal{A}}^T Q_{\check{x}\check{x}} l_{\mathcal{A}^\perp} = l_{\mathcal{A}}^T Q_{\hat{x}\hat{x}} l_{\mathcal{A}^\perp} = 0$. Applying the error propagation law to the solutions of (28), the gain number (25) would then take the following form

$$\gamma(l) = \frac{l_{\mathcal{A}}^T Q_{\hat{x}\hat{x}} l_{\mathcal{A}} + l_{\mathcal{A}^\perp}^T Q_{\hat{x}\hat{x}} l_{\mathcal{A}^\perp}}{l_{\mathcal{A}}^T Q_{\check{x}\check{x}} l_{\mathcal{A}} + l_{\mathcal{A}^\perp}^T Q_{\hat{x}\hat{x}} l_{\mathcal{A}^\perp}} \tag{29}$$

The variance $l_{\mathcal{A}^\perp}^T Q_{\check{x}\check{x}} l_{\mathcal{A}^\perp}$ is replaced by its float version $l_{\mathcal{A}^\perp}^T Q_{\hat{x}\hat{x}} l_{\mathcal{A}^\perp}$ in the denominator of (29), because of the identity $l_{\mathcal{A}^\perp}^T \check{x} = l_{\mathcal{A}^\perp}^T \hat{x}$.
According to (29), by choosing the linear function $l^T x$ such that $l_{\mathcal{A}} = 0$ (i.e., $l = l_{\mathcal{A}^\perp}$), the gain number γ becomes

$$\gamma(l_{\mathcal{A}^\perp}) = 1 \tag{30}$$

This is what one would expect since the float solution $l_{\mathcal{A}^\perp}^T \hat{x}$ does not benefit from IAR, thus having its variance unchanged. On the other hand, choosing the linear function $l_{\mathcal{A}}^T \hat{x}$ reduces (29) to

$$\gamma(l_{\mathcal{A}}) = \frac{l_{\mathcal{A}}^T Q_{\hat{x}\hat{x}} l_{\mathcal{A}}}{l_{\mathcal{A}}^T Q_{\check{x}\check{x}} l_{\mathcal{A}}} \tag{31}$$

We now show that the gain number of any linear function of x is bounded by (30) and (31), that is

$$1 = \gamma(l_{\mathcal{A}^\perp}) \leq \gamma(l) \leq \gamma(l_{\mathcal{A}}) \tag{32}$$

To see this, we express the gain number (29) in terms of $\gamma(l_{\mathcal{A}})$. This yields

$$\gamma(l) = \gamma(l_{\mathcal{A}}) \times \frac{1}{r_x} \tag{33}$$

in which the *reduction factor* r_x is given by

$$r_x = \frac{1+\nu^2}{1+\frac{\nu^2}{\gamma(l_{\mathcal{A}})}}; \quad \text{with} \quad \nu^2 = \frac{l_{\mathcal{A}^\perp}^T Q_{\check{x}\check{x}} l_{\mathcal{A}^\perp}}{l_{\mathcal{A}}^T Q_{\check{x}\check{x}} l_{\mathcal{A}}} \tag{34}$$

As any gain number is never smaller than one, i.e., $\gamma(l_{\mathcal{A}}) \geq 1$, we have

$$1 + \nu^2 \geq 1 + \frac{\nu^2}{\gamma(l_{\mathcal{A}})}, \quad \text{or} \quad r_x \geq 1 \tag{35}$$

The reduction factor r_x is therefore never smaller than one. This, in combined with (33), proves the inequality $\gamma \leq \gamma(l_{\mathcal{A}})$.

The reduction factor r_x tells us how many times the gain number γ is smaller than its maximum value $\gamma(l_{\mathcal{A}})$. The gain number of γ reaches its maximum $\gamma(l_{\mathcal{A}})$ when $l = l_{\mathcal{A}}$. In this case, the reduction factor becomes $r_x = 1$. When $l = l_{\mathcal{A}^\perp}$, the gain number of γ reaches its minimum 1. In this case, we have $l_{\mathcal{A}} \to 0$ (or $\nu^2 \to \infty$), having the maximum reduction factor $r_x \to \gamma(l_{\mathcal{A}})$.

5.2 Geometrical interpretation

The second expression of (28), together with $l_{\mathcal{A}}^T Q_{\hat{x}\hat{x}} l_{\mathcal{A}^\perp} = 0$, implies that

$$\begin{aligned} \left[\left(l_{\mathcal{A}}^T Q_{\hat{x}\hat{x}} l_{\mathcal{A}}\right)^{-1} l_{\mathcal{A}}^T Q_{\hat{x}\hat{x}}\right] l &= 1 \\ \left[\left(l_{\mathcal{A}^\perp}^T Q_{\hat{x}\hat{x}} l_{\mathcal{A}^\perp}\right)^{-1} l_{\mathcal{A}^\perp}^T Q_{\hat{x}\hat{x}}\right] l &= 1 \end{aligned} \tag{36}$$

From a geometrical point of view, the vectors $l_{\mathcal{A}}$ and $l_{\mathcal{A}^\perp}$ are thus the orthogonal *projections* of l. The magnitude of the gain number γ is driven by the 'direction' of the vector l (and not its length) with respect to the orthogonal projections $l_{\mathcal{A}}$ and $l_{\mathcal{A}^\perp}$. The gain number γ gets closer to its maximum $\gamma(l_{\mathcal{A}})$, the smaller the angle between l and $l_{\mathcal{A}}$. When l is orthogonal to the subspace $\mathcal{A}$ (i.e., $l = l_{\mathcal{A}^\perp}$), the gain number γ reaches its minimum $\gamma(l_{\mathcal{A}^\perp}) = 1$.

In the following, we present the gain numbers of the GNSS parameters in Table 1, using the representation (33). To get a better understanding of their variations, a 'geometric' approach is taken, for which the following geometrical concepts are used. We use the orthogonal projectors (cf. 14)

$$\begin{aligned} &\text{Between-satellite SD projection}: \mathcal{P}_{D_m} = D_m D_m^+ \\ &\text{Between-receiver SD projection}: \mathcal{P}_{D_n} = D_n D_n^+ \end{aligned} \tag{37}$$

Table 2 The (co)variance-type scalars used in the expressions of the gain numbers

Analytical expressions	GPS (L1/L2) example
Float: $Q_{[\hat{\rho},\hat{\imath}]} = \begin{bmatrix} c_{\hat{\rho}}^2 & c_{\hat{\rho}\hat{\imath}} \\ c_{\hat{\rho}\hat{\imath}} & c_{\hat{\imath}}^2 \end{bmatrix} = \left([e,\mu]^T C_p^{-1}[e,\mu]\right)^{-1}$	$\begin{bmatrix} 59.6^2, & -50.3^2 \\ -50.3^2, & 43.7^2 \end{bmatrix}$ (cm^2)
Fixed: $Q_{[\check{\rho},\check{\imath}]} = \begin{bmatrix} c_{\check{\rho}}^2 & c_{\check{\rho}\check{\imath}} \\ c_{\check{\rho}\check{\imath}} & c_{\check{\imath}}^2 \end{bmatrix} = \left(\begin{bmatrix} e & -\mu \\ e & +\mu \end{bmatrix}^T \begin{bmatrix} C_\phi^{-1} & 0 \\ 0 & C_p^{-1} \end{bmatrix} \begin{bmatrix} e & -\mu \\ e & +\mu \end{bmatrix} \right)^{-1}$	$\begin{bmatrix} 5.9^2, & 5.0^2 \\ 5.0^2, & 4.4^2 \end{bmatrix}$ [mm^2]

Their dual-frequency versions, i.e., $Q_{[\hat{\rho}_2,\hat{\imath}_2]}$, that are indicated in text by $(.)_2$, are computed based on the first two frequencies $j = 1, 2$. The GPS (L1/L2) example follows by setting $C_\phi = \sigma_\phi^2 I_2$, $C_p = \sigma_p^2 I_2$, with $\mu_1 = 1$ and $\mu_2 \approx 1.6469$ ($\sigma_\phi = 0.002$ [m], $\sigma_p = 0.2$ [m])

$c_{\hat{\imath}|\rho}^2 = c_{\hat{\imath}}^2 - (c_{\hat{\rho}\hat{\imath}}/c_{\hat{\rho}})^2$; $c_{\check{\imath}|\rho}^2 = c_{\check{\imath}}^2 - (c_{\check{\rho}\check{\imath}}/c_{\check{\rho}})^2$; $Q = \Lambda^{-1}\left(C_\phi + [e,-\mu]Q_{[\hat{\rho},\hat{\imath}]}[e,-\mu]^T\right)\Lambda^{-1}$, $Q_{|\rho} = \Lambda^{-1}\left(C_\phi + c_{\hat{\imath}|\rho}^2 \mu\mu^T\right)\Lambda^{-1}$

$Q_2 = \Lambda^{-1}\left(C_\phi + [e,-\mu]Q_{[\hat{\rho}_2,\hat{\imath}_2]}[e,-\mu]^T\right)\Lambda^{-1}$

The projector $\mathcal{P}_{D_m}$ projects any vector in $\mathbb{R}^m$ onto the subspace containing between-satellite SD functions. In case of $\mathcal{P}_{D_m}$, the orthogonality is defined by the metric $C_S \in \mathbb{R}^{m\times m}$, while the orthogonality of $\mathcal{P}_{D_n}$ is defined by the metric $C_R \in \mathbb{R}^{n\times n}$ (cf. 11). These two projectors structure the higher-dimension DD projector

$$\text{DD projection}: \quad \mathcal{P}_{DD} = \mathcal{P}_{D_n} \otimes \mathcal{P}_{D_m} \tag{38}$$

with the metric $C_R \otimes C_S \in \mathbb{R}^{mn\times mn}$. The projector $\mathcal{P}_{DD}$ orthogonally projects vector $l \in \mathbb{R}^{mn}$ onto the subspace containing the DD functions. The angle between vector l and its orthogonal projection $l_{DD} = \mathcal{P}_{DD}\, l$ is denoted by '$\measuredangle_{l_{DD}}^{l}$'. The (co)variance-type scalars, given in Table 2, frequently appear in our gain-number expressions.

5.3 Ionospheric parameters $\tilde{\imath}_r^s$

As shown in Fig. 5, the ionospheric parameters $\tilde{\imath}_R^S$ benefit from IAR through their DD components $\tilde{\imath}_{1R}^{1S}$. Thus, the role of subspace $\mathcal{A}$, in (33), is taken by the DD functions (i.e., $\mathcal{A} \mapsto DD$). We first present the maximum gain number $\gamma(l_{DD})$ and then evaluate its reduction factor r_χ. The $m \times n$ matrix $\tilde{\imath}_R^S$ is expressed in its vector form as $\text{vec}(\tilde{\imath}_R^S) \in \mathbb{R}^{mn}$.

Lemma 1 (Maximum gain number of $\tilde{\imath}_R^S$) *Given the observation Eq. (10), let $\hat{\tilde{\imath}}_R^S$ be the float solutions of the ionospheric parameters at epoch k that are obtained by the data of k epochs ($i = 1, \ldots, k$). Among the solutions $l^T \text{vec}(\hat{\tilde{\imath}}_R^S)$, the DD functions*

$$l_{DD}^T \,\text{vec}\left(\hat{\tilde{\imath}}_R^S\right), \quad \textit{with} \quad l_{DD} = \mathcal{P}_{DD}\, l, \tag{39}$$

achieve the maximum gain number

$$\gamma(l_{DD}) = \alpha_\iota\, \gamma^{GF} + (1-\alpha_\iota)\gamma^{GFi} \tag{40}$$

The geometry-free (GF) and geometry-fixed (GFi) gain numbers are, respectively, given as

$$\begin{aligned} \gamma^{GF} &= \tfrac{k-1}{k} + \tfrac{1}{k}\left(\frac{c_{\hat{\imath}}^2}{c_{\check{\imath}}^2}\right) \\ \gamma^{GFi} &= \tfrac{k-1}{k} + \tfrac{1}{k}\left(\frac{c_{\hat{\imath}|\rho}^2}{c_{\check{\imath}|\rho}^2}\right) \end{aligned} \tag{41}$$

The scalar $\alpha_\iota = [1 + (c_{\hat{\imath}|\rho}^2/c_{\hat{\imath}}^2)\tan^2(\psi_\iota)]^{-1}$ is specified by the deviation angle ψ_ι as follows

$$\psi_\iota = \measuredangle_{l_{D_\rho}}^{l_{DD}}, \quad l_{D_\rho} = \mathcal{P}_{D_\rho}\, l_{DD} \tag{42}$$

The orthogonal projector $\mathcal{P}_{D_\rho}$ projects onto the range-space of the design matrix of $\tilde{\rho}_{1R}^{1S}$ (see (82) in Appendix for its expression).

Proof See "Appendix". □

The above lemma shows, among the functions of the ionospheric parameters, that the DD functions of $\hat{\tilde{\imath}}_R^S$ achieve the largest gain number due to ambiguity fixing. The value is a *convex* combination of γ^{GF} and γ^{GFi}. When $k = 1$ (i.e., single-epoch), both of these gain numbers represent large values (see Table 2)

$$\begin{aligned} \gamma^{GF} &\overset{k=1}{=} \frac{c_{\hat{\imath}}^2}{c_{\check{\imath}}^2} \approx 99.3^2 \\ \gamma^{GFi} &\overset{k=1}{=} \frac{c_{\hat{\imath}|\rho}^2}{c_{\check{\imath}|\rho}^2} \approx 103.9^2 \end{aligned} \tag{43}$$

affirming the two orders of magnitude improvement by IAR. They decrease as the number of epochs k increases, tending to '1' when $k \to \infty$. The 'geometry-free' gain number γ^{GF} corresponds to the case where the non-dispersive parameter ρ_R^S is not parametrized into the position/ZTD increments Δx_R. Thus, no information about the relative receiver-satellite geometry is present in the model's design matrix. On the other hand, the 'geometry-fixed' gain number γ^{GFi} corresponds to the case where the position/ZTD

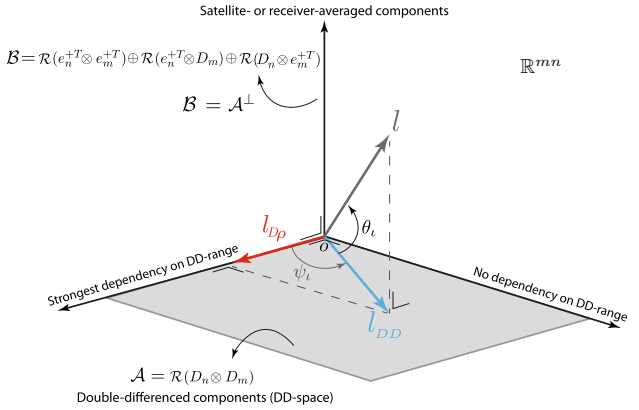

Fig. 8 Geometrical illustration showing the relation between vector $l \in \mathbb{R}^{m\times n}$ (black) and its orthogonal projections l_{DD} (blue) and l_{D_ρ} (red). The gray plain represents the subspace containing all DD ionospheric functions. The axis orthogonal to l_{D_ρ} shows the subspace containing the DD ionospheric functions that are uncorrelated with $\hat{\check{\rho}}^{1S}_{1R}$, having no dependency on the DD-range solutions. The 'direct sum' between two subspaces is denoted by $\oplus$

parameters are completely known, i.e., $\Delta\check{x}_R = 0$. Thus, the full information on the receiver-satellite geometry is given.

The maximum gain number $\gamma(l_{DD})$ ranges between γ^{GF} and γ^{GFi} through the scalar $0 \le \alpha_\iota \le 1$. The scalar α_ι itself is driven by the deviation angle ψ_ι. This angle measures the *dependency* of solution $l^T_{DD}\,\mathrm{vec}(\hat{\check{\imath}}^S_R)$ on the DD-range solution $\hat{\check{\rho}}^{1S}_{1R}$. When $\psi_\iota = 90°$, the vector l_{DD} is orthogonal to the design matrix of the DD-range solution, thus having $l^T_{DD}\,\mathrm{vec}(\hat{\check{\imath}}^S_R)$ *uncorrelated* with $\hat{\check{\rho}}^{1S}_{1R}$, and $\alpha_\iota = 0$. In this case, the solution $l^T_{DD}\,\mathrm{vec}(\hat{\check{\imath}}^S_R)$ has no dependency on the DD-range solution, thereby having the gain number equal to the geometry-fixed one, i.e., $\gamma(l_{DD}) = \gamma^{GFi}$. When $\psi_\iota = 0$, the vector l_{DD} lies in the range-space of the design matrix of the DD-range solution, having $l^T_{DD}\,\mathrm{vec}(\hat{\check{\imath}}^S_R)$ with maximum dependency on $\hat{\check{\rho}}^{1S}_{1R}$, and $\alpha_\iota = 1$. In this case, the solution $l^T_{DD}\,\mathrm{vec}(\hat{\check{\imath}}^S_R)$ therefore has the gain number equal to the geometry-free one, i.e., $\gamma(l_{DD}) = \gamma^{GF}$.

The corresponding geometrical illustration is presented in Fig. 8. The gray plain represents the subspace containing all DD ionospheric functions. When vector l_{DD} coincides with its projection l_{D_ρ}, the deviation angle becomes $\psi_\iota = 0$. The float solution $l^T_{DD}\,\mathrm{vec}(\hat{\check{\imath}}^S_R)$ would then experience strongest dependency on the DD-range solution. The axis orthogonal to l_{D_ρ} shows the subspace containing the DD ionospheric functions that are uncorrelated with the DD-range solution, thereby having no dependency on $\hat{\check{\rho}}^{1S}_{1R}$.

Note that the solutions $l^T\mathrm{vec}(\hat{\check{\imath}}^S_R)$ do not only represent the DD components. That is why the vector l does not lie in the DD space (see Fig. 8). The deviation angle θ_ι governs the reduction in the maximum gain number $\gamma(l_{DD})$. Below, the corresponding reduction factor is presented.

Lemma 2 (Gain number of $\check{\imath}^S_R$) *Given the observation Eq. (10), let $\hat{\check{\imath}}^S_R$ be the float solutions of the ionospheric parameters at epoch k that are obtained by the data of k epochs ($i = 1,\ldots,k$). The gain number of the float solution $l^T\mathrm{vec}(\hat{\check{\imath}}^S_R)$ is linked to its maximum $\gamma_{\check{\imath}^S_R}(l_{DD})$ through*

$$\gamma(l) = \gamma(l_{DD}) \times \frac{1}{r_x} \tag{44}$$

in which the reduction factor r_x is given by

$$r_x = \frac{1 + \nu_\iota^2 \tan^2(\theta_\iota)}{1 + \left[\nu_\iota^2/\gamma(l_{DD})\right]\tan^2(\theta_\iota)} \tag{45}$$

with the scalar $\nu_\iota^2 = [(c_{\check{\imath}}^2/c_{\check{\imath}_2}^2) + (c_{\check{\imath}|\rho}^2/c_{\check{\imath}_2}^2)\tan^2(\psi_\iota)]^{-1}$ and the deviation angle $\theta_\iota = \measuredangle^{l}_{l_{DD}}$.

Proof See "Appendix". □

When $\theta_\iota = 0$, the solution $l^T\mathrm{vec}(\hat{\check{\imath}}^S_R)$ belongs to the class of DD functions. In that the case, there is no reduction in the maximum gain number $\gamma(l_{DD})$, i.e., $r_x = 1$. When vector l is orthogonal to the DD space (i.e., $\theta_\iota = 90°$), the solution $l^T\mathrm{vec}(\hat{\check{\imath}}^S_R)$ represents the satellite- or receiver-averaged functions (Fig. 8). In this case, the solution $l^T\mathrm{vec}(\hat{\check{\imath}}^S_R)$ becomes uncorrelated with DD float ambiguities, having the maximum reduction factor $r_x = \gamma(l_{DD})$. Thus, $\gamma = 1$.

Figure 9 shows square-root gain numbers of the ionospheric solutions $l^T\mathrm{vec}(\hat{\check{\imath}}^S_R)$ as a function of the deviation angle θ_ι. As shown, the gain number significantly decreases as θ_ι gets closer to 90°. The deviation angles corresponding to the UD component $\check{\imath}^s_r$, between-receiver (BR) SD component $\check{\imath}^s_{1r}$ and between-satellite (BS) SD component $\check{\imath}^{1s}_r$ can be evaluated as functions of the numbers of satellites and receivers m and n as follows (see "Appendix")

$$\cos^2(\theta_\iota) = \begin{cases} \left(1-\frac{1}{n}\right)\left(1-\frac{1}{m}\right), & \text{UD} \\ \left(1-\frac{1}{m}\right), & \text{BR-SD} \\ \left(1-\frac{1}{n}\right), & \text{BS-SD} \end{cases} \tag{46}$$

The larger the numbers m and n, the smaller the deviation angle θ_ι becomes. For the numbers of receivers $2 \le n \le 300$, and numbers of satellites $5 \le m \le 60$, the ranges of θ_ι have been highlighted in Fig. 9. As shown, the standard deviation of the float solution $\hat{\check{\imath}}^s_r$ decreases by factors of 1 to 7. Depending on the numbers of receivers and satellites, the standard deviation of $\hat{\check{\imath}}^s_{1r}$ and $\hat{\check{\imath}}^{1s}_r$ can, respectively, become up to 8 and 19 times smaller after IAR. These standard deviation ratios get smaller, the larger the number of epochs k. This shows that the float solutions of the ionospheric components can have very distinct responses to IAR.

To conclude this subsection, it is important to remark that the DD functions $\check{\imath}^{1S}_{1R}$ refer to those functions at one individual

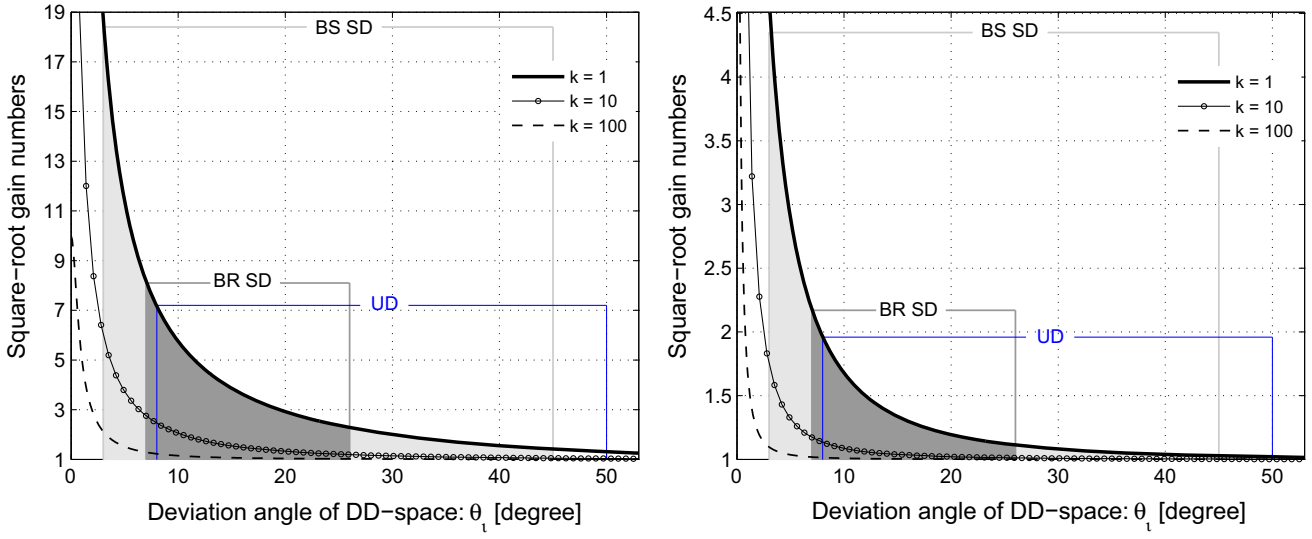

Fig. 9 Square-root gain numbers of the ionospheric solutions $l^T \mathrm{vec}(\hat{\tilde{t}}^S_R)$ as a function of the deviation angle θ_ι. *Left*: the geometry-free scenario ($\psi_\iota = 0$), *right*: the geometry-fixed scenario ($\psi_\iota = 90°$). The ranges of the deviation angles corresponding to the UD component $\tilde{t}^s_r$ (bounded by the blue lines), between-receiver (BR) SD component $\tilde{t}^s_{1r}$ (dark gray area) and between-satellite (BS) SD component $\tilde{t}^{1s}_r$ (light gray area) are highlighted

epoch k (cf. Lemma 1). These functions should therefore *not* to be confused with their *between-epoch* differenced counterparts. As shown, for instance in (Khodabandeh and Teunissen 2016), any sole function of the 'between-epoch' differenced components are uncorrelated with the DD float ambiguities and therefore does not benefit from IAR. The same conclusion holds for the other DD functions.

5.4 Clock parameters $d\tilde{t}_r$ and $d\tilde{t}^s$

According to Fig. 5, the satellite clock parameters $d\tilde{t}^S$ benefit from IAR through their SD components $d\tilde{t}^{1S}$. Thus, the role of subspace $\mathcal{A}$, in (33), is now taken by the between-satellite SD functions. Similar to the ionospheric parameters, we first present the maximum gain number $\gamma(l_{D_m})$.

Lemma 3 (Maximum gain number of $d\tilde{t}^S$) *Given the observation Eq. (10), let $d\hat{\tilde{t}}^S$ be the float solutions of the satellite clock parameters at epoch k that are obtained by the data of k epochs ($i = 1, \ldots, k$). Among the solutions $l^T d\hat{\tilde{t}}^S$, the SD functions*

$$l^T_{D_m} d\hat{\tilde{t}}^S_R, \quad \textit{with} \quad l_{D_m} = \mathcal{P}_{D_m} l, \tag{47}$$

achieve the maximum gain number

$$\gamma(l_{D_m}) = \alpha_{dt}\, \gamma^{GF} + (1 - \alpha_{dt})\gamma^{GFi} \tag{48}$$

The geometry-free (GF) and geometry-fixed (GFi) gain numbers are, respectively, introduced as

$$\begin{aligned} \gamma^{GF} &= 1 + \tfrac{n-1}{k}\left[\frac{\left(c^2_{\hat{\rho}}/c^2_{\check{\rho}}\right)-1}{n+\left(c^2_{\hat{\rho}_2}/c^2_{\check{\rho}}\right)-1}\right] \\ \gamma^{GFi} &= 1 \end{aligned} \tag{49}$$

The scalar $\alpha_{dt} = [1+(\frac{c^2_{\hat{\rho}_2}}{c^2_{\hat{\rho}_2}+(n-1)c^2_{\check{\rho}}})\tan^2(\psi_{dt})]^{-1}$ is specified by the deviation angle ψ_{dt} as follows

$$\psi_{dt} = \measuredangle^{l_{D_m}}_{l_{D_{m\rho}}}, \quad l_{D_{m\rho}} = \mathcal{P}_{D_{m\rho}}\, l_{D_m} \tag{50}$$

The orthogonal projector $\mathcal{P}_{D_{m\rho}}$ projects onto the range-space of the design matrix of $\tilde{\rho}^{1S}_{1\check{r}}$ (see (77) in "Appendix" for its expression).

Proof See "Appendix". □

Note the resemblance between (48) and its ionospheric counterpart (40). The maximum gain number $\gamma(l_{D_m})$ is also a convex combination of γ^{GF} and γ^{GFi}. In contrast to the ionospheric gain numbers (43) where both represent very large values (i.e., around 100^2), the values of the GF and GFi gain numbers of the satellite clock parameters can be quite different. For the geometry-fixed case, we have $\gamma^{GFi} = 1$ as the dependency of the clock solutions $l^T d\hat{\tilde{t}}^S$ on the position/ZTD components $\Delta\tilde{x}_R$ is absent (cf. Fig. 5). For the geometry-free case, however, we have

$$\gamma^{GF} \leq 1 + \frac{n-1}{k} \overset{k=1}{=} n \tag{51}$$

The above upper-bound is sharp when the number of receivers n is not too large. The larger the number of network receivers, the larger the precision gain the satellite clock solutions achieve after IAR. In the single-epoch case, the GF gain number roughly becomes n. This can be well understood from the satellite clocks' constituent components as follows (Fig. 5 with $\Delta\tilde{x}_1 = 0$)

$$\begin{aligned} \text{Float}: \quad & d\hat{\tilde{t}}^{1s} = -\hat{\tilde{\rho}}_{\tilde{r}}^{1s} + \hat{\rho}_{1\tilde{r}}^{1s} = -\hat{\tilde{\rho}}_{1}^{1s} \\ \text{Fixed}: \quad & d\check{\tilde{t}}^{1s} = -\hat{\tilde{\rho}}_{\tilde{r}}^{1s} + \check{\rho}_{1\tilde{r}}^{1s} \end{aligned} \tag{52}$$

As the variance of the fixed solution $\check{\rho}_{1\tilde{r}}^{1s}$ is negligible compared to that of $\hat{\tilde{\rho}}_{\tilde{r}}^{1s}$ (for not too large n), one can then conclude that

$$\mathsf{D}(d\check{\tilde{t}}^{1s}) \approx \mathsf{D}\left(-\hat{\tilde{\rho}}_{\tilde{r}}^{1s}\right) = \tfrac{1}{n}\mathsf{D}\left(-\hat{\tilde{\rho}}_{1}^{1s}\right) = \tfrac{1}{n}\mathsf{D}\left(d\hat{\tilde{t}}^{1s}\right) \tag{53}$$

The maximum gain number $\gamma(l_{D_m})$ ranges between γ^{GFi} and γ^{GF} through the scalar $0 \leq \alpha_{dt} \leq 1$ which itself is driven by the deviation angle ψ_{dt}. This angle measures the *dependency* of solution $l^T d\hat{\tilde{t}}^S$ on the DD-range solution $\hat{\tilde{\rho}}_{1\tilde{r}}^{1S}$, thereby its dependency on the strength of the model's geometry. Figure 10 shows square root of the maximum gain numbers of the satellite clock solutions, i.e., $\gamma(l_{D_m})$, as a function of the deviation angle ψ_{dt}. When $\psi_{dt} = 0$ (geometry-free case), the model's geometry is weakest, having the solutions $l^T d\hat{\tilde{t}}^S$ with largest precision gains due to ambiguity fixing. The precision gains decrease as the deviation angle ψ_{dt} gets closer to 90° (i.e., the model's geometry gets stronger). In the extreme case $\psi_{dt} = 90°$ (geometry-fixed case), the model's geometry becomes strongest. In this case, no precision improvement is gained after IAR, as the clock solutions $l^T d\hat{\tilde{t}}^S$ would then be uncorrelated with the DD float ambiguities.

Since the solutions $l^T d\hat{\tilde{t}}^S$ do not only represent the SD components, a nonzero deviation angle, say θ_{dt}, from the SD-space can further reduce the maximum gain number $\gamma(l_{D_m})$.

Lemma 4 (Gain number of $d\tilde{t}^S$) *Given the observation Eq. (10), let $d\hat{\tilde{t}}^S$ be the float solutions of the satellite clock parameters at epoch k that are obtained by the data of k epochs $(i = 1, \ldots, k)$. The gain number of the float solution $l^T d\hat{\tilde{t}}^S$ is linked to its maximum $\gamma(l_{D_m})$ through*

$$\gamma(l) = \gamma(l_{D_m}) \times \frac{1}{r_x} \tag{54}$$

in which the reduction factor r_x is given by

$$r_x = \frac{1 + v_{dt}^2 \tan^2(\theta_{dt})}{1 + [v_{dt}^2/\gamma(l_{D_m})]\tan^2(\theta_{dt})} \tag{55}$$

with the scalar $v_{dt}^2 = n[1 + (n-1)(c_{\tilde{\rho}}^2/c_{\hat{\rho}_2}^2)\cos^2(\psi_{dt})]^{-1}$ and the deviation angle $\theta_{dt} = \measuredangle_{l_{D_m}}^{l}$.

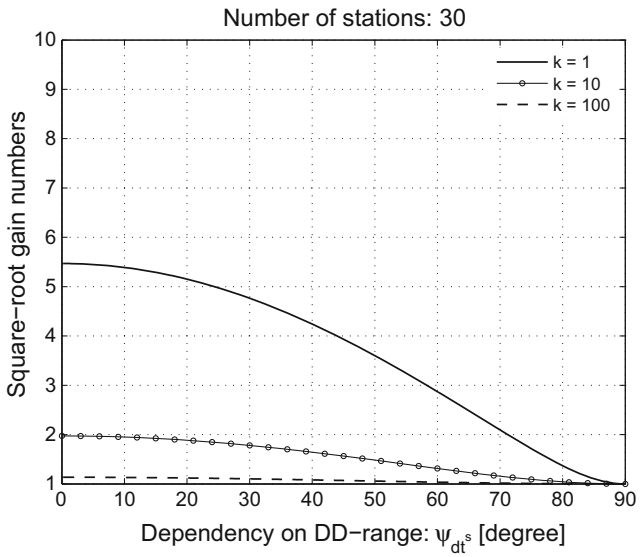

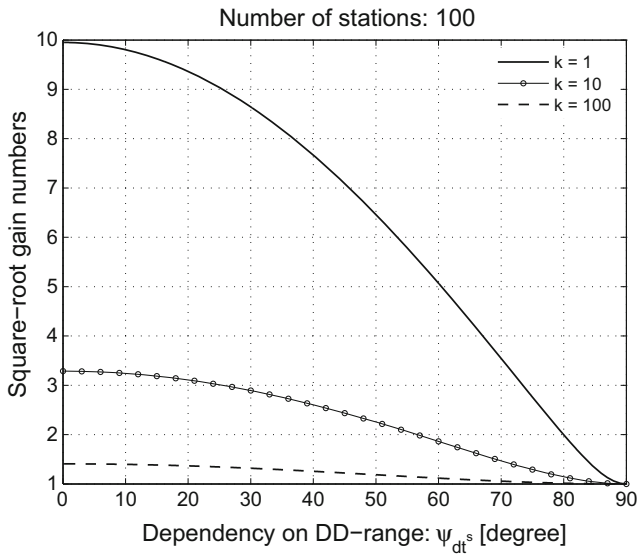

Fig. 10 Square root of the maximum gain numbers of the satellite clock solutions $l^T(d\hat{\tilde{t}}^S)$ as a function of the deviation angle ψ_{dt}. This angle measures the *dependency* of solution $l^T d\hat{\tilde{t}}^S$ on the strength of the model's geometry. *Left*: A network of $n = 30$ receivers, *right*: a network of $n = 100$ receivers. The precision gains decrease as the deviation angle ψ_{dt} gets closer to 90^0 (i.e., the model's geometry gets stronger)

Proof See "Appendix". □

The reduction factor r_x, in (55), shows how the maximum gain number (54) reduces when the float solution $l^T d\hat{\check{t}}^S$ deviates from the class of between-satellite SD functions. For the geometry-free case, square-root gain numbers of the satellite clock solutions $l^T d\hat{\check{t}}^S$ as a function of the deviation angle θ_{dt} is shown (Fig. 11). The values decrease as the deviation angle θ_{dt} increases. Similar to (46), the deviation angles corresponding to the UD component $d\tilde{t}^s$ can be evaluated (see "Appendix")

$$\cos^2(\theta_{dt}) = 1 - \frac{1}{m} \tag{56}$$

Thus, when the number of satellites gets larger, the deviation angle θ_{dt} gets closer to zero. In this case, the UD clock solution $d\hat{\tilde{t}}^s$ can significantly benefit from IAR. For the numbers of satellites $5 \leq m \leq 60$, the ranges of θ_{dt} are depicted in Fig. 11. Accordingly, the standard deviation of the float solution $d\hat{\tilde{t}}^s$ decreases by factors of 2 to 6 when the model's geometry is weakest (i.e., the geometry-free case).
Let us now consider the receiver clock solutions $d\hat{\tilde{t}}_R$.

Lemma 5 (Gain number of $d\tilde{t}_R$) *Given the observation Eq. (10), let $d\hat{\tilde{t}}_R$ be the float solutions of the receiver clock parameters at epoch k that are obtained by the data of k epochs ($i = 1, \ldots, k$). The gain number of the float solution $l^T d\hat{\tilde{t}}_R$ is given by*

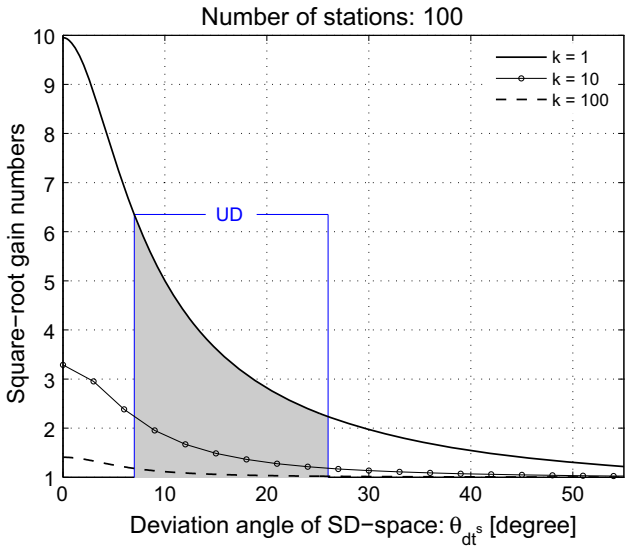

Fig. 11 Square-root gain numbers of the satellite clock solutions $l^T d\hat{\check{t}}^S$ as a function of the deviation angle θ_{dt}, for the geometry-free scenario ($\psi_l = 0$) and a network of $n = 100$ receivers. The ranges of the deviation angles corresponding to the UD component $d\tilde{t}^s$ (gray area) are also given

$$\gamma(l) = 1 + \frac{1}{k}\left[\frac{c_{\hat{\rho}}^2 - c_{\check{\rho}}^2}{c_{\hat{\rho}_2}^2 \tan^2(\psi_g) + c_{\check{\rho}}^2}\right] \tag{57}$$

with the deviation angle

$$\psi_g = \measuredangle_g^{e_m^{+T}}, \quad g = \mathcal{P}_G\, e_m^{+T} \tag{58}$$

The orthogonal projector $\mathcal{P}_G$ projects onto the range-space of $C_S^{-1} G_1^S$ (see "Appendix" for its expression).

Proof See "Appendix". □

The above lemma shows that the receiver clock gain number γ does not depend on vector l and therefore on the choice of function $l^T d\tilde{t}_R$. This is due to the fact that the estimable receiver clocks $d\tilde{t}_r$ are of a between-receiver SD nature (cf. Table 1). Similar to the satellite clocks, their maximum gain number is experienced for the SD functions and thus not dependent on the choice of l. That is why no reduction factor is devised for the solutions $l^T d\hat{\tilde{t}}_R$.

Next to the number of epochs k, the gain number (57) is driven by the deviation angle ψ_g. The angle ψ_g measures the dependency of the vector e_m on the matrix of receiver-satellite direction vectors $G_1 = [g_1^1, \ldots, g_1^m]^T$. We now consider two extreme cases. First consider the case where $\psi_g = 0$, i.e., $\tan(\psi_g) = 0$. The gain number (57) is reduced to (see Table 2)

$$\gamma(l) = 1 + \frac{1}{k}\left[\frac{c_{\hat{\rho}}^2}{c_{\check{\rho}}^2} - 1\right] \overset{k=1}{=} \frac{c_{\hat{\rho}}^2}{c_{\check{\rho}}^2} \approx 101^2 \tag{59}$$

The extreme case $\psi_g = 0$ occurs when e_m is completely dependent on G_1. In this case, the design matrix $[e_m, G_1]$ is singular. Thus, when the receiver clocks $d\tilde{t}_R$ are poorly estimable, they significantly benefit from IAR. Now consider the second extreme case when $\psi_g = 90°$, i.e., $\tan(\psi_g) \to \infty$. The gain number (57) is reduced to $\gamma \to 1$. The condition $\psi_g = 90°$ occurs when the vector e_m is orthogonal to the receiver-satellite direction matrix G_1 (with metric C_S^{-1}), i.e., when the float solutions $d\hat{\tilde{t}}_R$ are uncorrelated with the float baseline/ZTD solutions $\Delta\tilde{x}_R$. This is in agreement with the qualitative analysis done in Sect. 4 (cf. Fig. 5). Similar to the satellite clocks, the receiver clocks' precision gain due to ambiguity fixing is therefore large when the model's geometry is weak.

5.5 Phase biases $\tilde{\delta}_{r,j}$ and $\tilde{\delta}^s_{,j}$

For each receiver and satellite, we have f number of phase biases $\tilde{\delta}_{r,j}$ and $\tilde{\delta}^s_{,j}$ ($j = 1, \ldots, f$), respectively. Their multivariate forms, respectively, read $\tilde{\delta}_R \in \mathbb{R}^{f\times n}$ and $\tilde{\delta}^S \in \mathbb{R}^{fm}$. We consider the gain number of their 'between-frequency'

combinations characterized by the f-vector q. If there is no reason for confusion, we therefore refer to the following functions

$$\begin{aligned} &\text{Satellite phase biases}: \quad (q^T \otimes l^T)\hat{\tilde{\delta}}^S, \quad l \in \mathbb{R}^m \\ &\text{Receiver phase biases}: \quad q^T \hat{\tilde{\delta}}_R\, l, \qquad\quad l \in \mathbb{R}^n \end{aligned} \tag{60}$$

as the float solutions of the phase biases. Next to the vector l, their gain numbers are thus also dependent on the vector q. The corresponding gain numbers are presented below.

Lemma 6 (Gain numbers of $\tilde{\delta}^S$ and $\tilde{\delta}_R$) *Given the observation Eq. (10), let $\tilde{\delta}^S$ be the float solutions of the satellite phase biases at epoch k that are obtained by the data of k epochs ($i = 1, \ldots, k$). The gain numbers of (60) are, respectively, given as*

$$\begin{aligned} \gamma(l) &= \gamma(l_{D_m}) \times \frac{1}{r_x}, \quad l \in \mathbb{R}^m \\ \gamma(l) &= \gamma_{\tilde{\delta}_R}, \quad l \in \mathbb{R}^n \end{aligned} \tag{61}$$

with the reduction factor

$$r_x = \frac{1 + n\tan^2(\theta_{dt})}{1 + [n/\gamma(l_{D_m})]\tan^2(\theta_{dt})} \tag{62}$$

and

$$\begin{aligned} \gamma(l_{D_m}) &= \cos^2(\psi_{dt})\,\gamma_{\tilde{\delta}S}^{GF} + \sin^2(\psi_{dt})\gamma_{\tilde{\delta}S}^{GFi} \\ \gamma_{\tilde{\delta}_R} &= \cos^2(\psi_1)\,\gamma_{\tilde{\delta}_R}^{GF} + \sin^2(\psi_1)\gamma_{\tilde{\delta}_R}^{GFi} \end{aligned} \tag{63}$$

The geometry-free (GF) and geometry-fixed (GFi) gain numbers are introduced as (see Table 2)

$$\begin{aligned} \gamma_{\tilde{\delta}S}^{GF} &= 1 + \tfrac{n-1}{k}\left[\tfrac{q^T Q q}{q^T Q_{2q} q}\right]; \quad \gamma_{\tilde{\delta}S}^{GFi} = 1 + \tfrac{n-1}{k}\left[\tfrac{q^T Q_{|\rho} q}{q^T Q_{2q} q}\right] \\ \gamma_{\tilde{\delta}_R}^{GF} &= 1 + \tfrac{1}{k}\left[\tfrac{q^T Q q}{q^T Q_{2q} q}\right]; \quad\quad \gamma_{\tilde{\delta}_R}^{GFi} = 1 + \tfrac{1}{k}\left[\tfrac{q^T Q_{|\rho} q}{q^T Q_{2q} q}\right] \end{aligned} \tag{64}$$

The deviation angle ψ_{dt} and θ_{dt} follow from (50) and (55), respectively. The deviation angle ψ_1 reads

$$\psi_1 = \measuredangle^{\mathcal{P}_{D_m} v_1}_{\mathcal{P}_{D_{m\rho}} v_1}, \quad v_1 = [1, 0, \ldots, 0]^T \tag{65}$$

Proof See "Appendix". □

Similar to the receiver clock gain number (57), the receiver phase-bias gain number does not depend on the vector l. This is due to the fact that the estimable receiver biases $\tilde{\delta}_{r,j}$ are of a between-receiver SD nature (cf. Table 1). Thus, no reduction factor is devised for the solutions $q^T \hat{\tilde{\delta}}_R\, l$. In case of the satellite phase-bias gain number, however, the reduction factor (62) is formulated to measure the reduction in the maximum value $\gamma(l_{D_m})$. The more the angle θ_{dt} deviates from the between-satellite SD functions, the larger the reduction factor r_x, thus the smaller the gain number γ becomes.

Both of the satellite and receiver phase-bias gain numbers can be expressed as a convex combinations of their GF and GFi counterparts (cf. 63). For the satellite phase biases, the *same* deviation angle ψ_{dt} as that of (50) is given. This angle measures the dependency of the phase-bias solutions on the DD-range solution $\hat{\tilde{\rho}}^{1S}_{1\bar{r}}$, thereby its dependency on the strength of the model's geometry. For the receiver phase biases, the deviation angle ψ_1 is given (cf. 65). This angle depends on the constant vector v_1 corresponding to the reference satellite $s = 1$. This dependency is driven by the choice of $\mathcal{S}$-basis (see the term $z^1_{1r,j}$ in $\tilde{\delta}_{r,j}$ of Table 1). This shows that a change in the model's $\mathcal{S}$-basis can change the interpretation of the receiver phase biases and ditto their precision gains.

Similar to its satellite clock counterpart (51), the geometry-free gain number $\gamma_{\tilde{\delta}S}^{GF}$, in (64), is bounded from above as

$$\gamma_{\tilde{\delta}S}^{GF} \leq 1 + \frac{n-1}{k} \overset{k=1}{=} n \tag{66}$$

The above upper-bound is reached for the dual-frequency case ($f = 2$) and is sharp when the number of receivers n is not too large. In the single-epoch case, the GF gain number becomes n. This can be understood from the satellite phase biases' constituent components as follows (Fig. 5)

$$\begin{aligned} &\text{Float}: \quad \hat{\tilde{\delta}}^{1s}_{,j} = -\hat{\tilde{a}}^{1s}_{\bar{r},j} + \hat{\tilde{a}}^{1s}_{1\bar{r},j} = -\hat{\tilde{a}}^{1s}_{1,j} \\ &\text{Fixed}: \quad \breve{\tilde{\delta}}^{1s}_{,j} = -\hat{\tilde{a}}^{1s}_{\bar{r},j} + \breve{a}^{1s}_{1\bar{r},j} \end{aligned} \tag{67}$$

The fixed solution $\breve{\rho}^{1s}_{1\bar{r}}$ has a zero variance (i.e., non-random). We therefore have

$$\mathsf{D}\left(\breve{\tilde{\delta}}^{1s}_{,j}\right) = \mathsf{D}\left(-\hat{\tilde{a}}^{1s}_{\bar{r},j}\right) = \tfrac{1}{n}\mathsf{D}\left(-\hat{\tilde{a}}^{1s}_{1,j}\right) = \tfrac{1}{n}\mathsf{D}\left(\hat{\tilde{\delta}}^{1s}_{,j}\right) \tag{68}$$

On the other hand, for the stochastic model $C_\phi = \sigma_\phi^2 I_f$ and $C_p = \sigma_p^2 I_f$, the geometry-fixed gain number $\gamma_{\tilde{\delta}S}^{GFi}$, in (64), is bounded from below as follows

$$1 \approx 1 + \frac{(n-1)}{k\left(\left[c^2_{\hat{\rho}_2}/c^2_{\hat{\rho}}\right] + \epsilon\right)}\epsilon \leq \gamma_{\tilde{\delta}S}^{GFi}, \quad \text{with} \quad \epsilon = \frac{\sigma_\phi^2}{\sigma_p^2} \tag{69}$$

Since the phase-to-code variance ratio ϵ is very small, the above lower-bound is close to 1. The lower-bound is reached for the 'between-frequency' phase-bias combinations that are *uncorrelated* with the DD float ionospheric solutions $\hat{\iota}^{1S}_{1R}$, i.e., those characterized by the choice $q = \Lambda(e_f - [c_{\hat{\rho}\hat{\iota}}/c^2_{\hat{\rho}}]\,\mu)$ (Table 2). The reason is as follows. For argument sake,

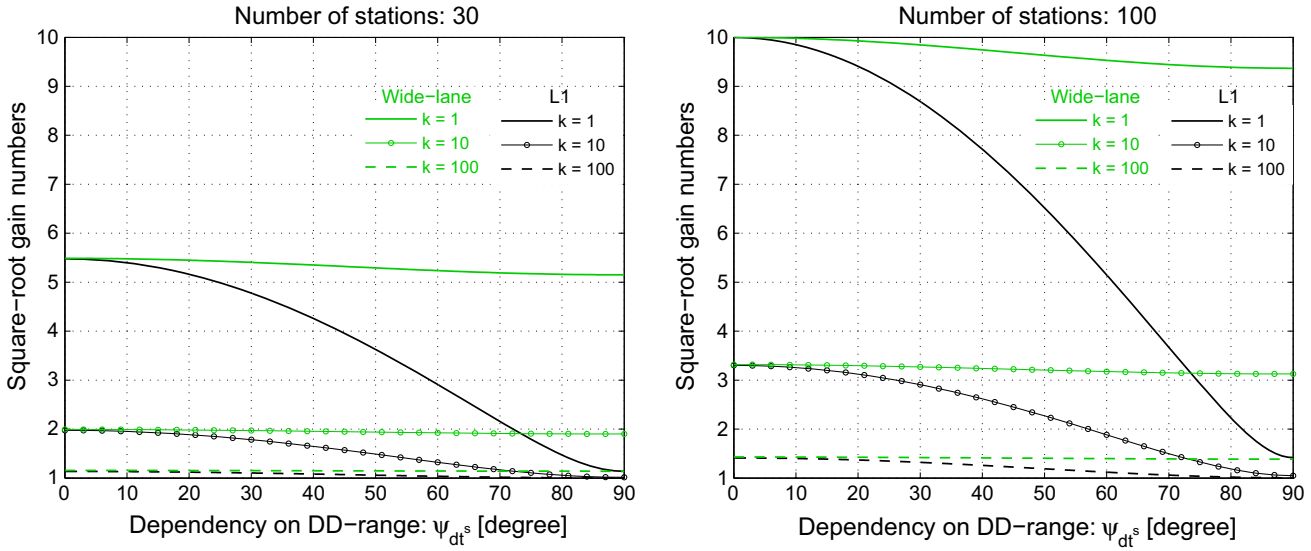

Fig. 12 Square root of the maximum gain numbers of the satellite phase biases (L1 in black, wide-lane in green) as a function of the deviation angle ψ_{dt}. This angle measures the *dependency* of the solutions on the strength of the model's geometry. *Left*: A network of $n = 30$ receivers, *right*: a network of $n = 100$ receivers. In case of L1 phase biases, the precision gains decrease as the deviation angle ψ_{dt} gets closer to 90° (i.e., the model's geometry gets stronger). In case of wide-lane phase biases, however, the precision gains are almost insensitive to the strength of the model's geometry and behave rather constant for different values of ψ_{dt}

assume that $\hat{\iota}^{1S}_{1R}$ are completely known. In the geometry-fixed case, the precision of the float ambiguities $\hat{\check{a}}^{1s}_{1\bar{r},j}$, in (67), would then already be at the phase-level, as both ρ^{1s}_{1r} and ι^{1s}_{1r} are absent in the DD model (2). Switching from $\hat{\check{\delta}}^{1s}_{,j}$ to $\check{\delta}^{1s}_{,j}$ would therefore only eliminate the randomness of $\hat{\check{a}}^{1s}_{1\bar{r},j}$ which is very small (see 67). Now assume that the DD ionosphere parameters ι^{1s}_{1r} are present. As the stated 'between-frequency' phase-bias combinations are uncorrelated with $\hat{\iota}^{1S}_{1R}$, the corresponding combinations of the float ambiguities $\hat{\check{a}}^{1s}_{1\bar{r},j}$ are of phase-level precision in the geometry-fixed case. Thus, small precision gain by these combinations is experienced after ambiguity fixing.

The bounds (66) and (69) show that the float phase bias solutions have different precision gains ranging from 1 (the geometry-fixed case) to the number of network receivers n (the geometry-free case). This may suggest, similar to the clock parameters, that the precision gain of the phase biases do also very much depend on the strength of the model's geometry. In Fig. 12 we plot square root of the maximum gain numbers of the satellite phase biases (L1 in black, wide-lane in green) as a function of the deviation angle ψ_{dt}. Compare the results with those in Fig. 10. While the L1 phase bias gain numbers have a similar behavior as that of the clock gain numbers, the wide-lane phase-bias gain numbers are almost insensitive to the strength of the model's geometry and behave rather constant for different values of ψ_{dt}. This follows from the term (see Table 2)

$$\frac{q^T Q_{|\rho} q}{q^T Q_2 q} \approx \begin{cases} 0.01, & q = [1,0]^T \quad \text{(L1)} \\ 0.88, & q = [1,-1]^T \ \text{(wide-lane)} \end{cases} \tag{70}$$

in the GFi expression (64). It shows, in case of L1 phase biases, that $\gamma^{GFi}_{\check{\delta}S}$ weakly depends on the number of receivers n and epochs k, i.e., $\gamma^{GFi}_{\check{\delta}S} \approx 1$. For the wide-lane phase biases, however, $\gamma^{GFi}_{\check{\delta}S}$ approximates its geometry-free counterpart $\gamma^{GF}_{\check{\delta}S}$. The conclusion reads therefore that there exist combinations of the phase biases, like the wide-lane ones, that can benefit from IAR irrespective of the model's strength.

6 Summary and concluding remarks

In this contribution, we introduced a novel four-block canonical decomposition of the multivariate GNSS model to analyze the IAR impact on the parameters (Fig. 3). The four-block decomposition allows one to address how the DD ambiguity-resolved phase data propagate into the estimable parameters, thereby enabling one to measure the precision gain of the parameters due to ambiguity fixing. Apart from the DD block, the three satellite- and/or receiver-averaged blocks are uncorrelated with DD float ambiguities, requiring code for their estimation even after IAR. It is the presence of these blocks that prohibits the precision gain of the other-than-DD functions to reach the two orders of magnitude level. Thus, any function of these three blocks remains *unaffected* by IAR. We employed this strategy and conducted a *qualitative* analysis with the following conclusions (cf. Fig. 5):

- *Estimable receiver and satellite code biases* do not depend on the DD block and therefore on the DD float ambiguities. These parameters do *not* benefit from IAR. If one is interested to determine such parameters, no extra ambiguity-fixing step is required.
- *Slant ionospheric parameters* benefit from IAR only through their DD components. For the short-baseline scenarios where the DD ionospheric delays are *a priori* known to be absent, the other components of the ionospheric parameters (e.g., UD and SD components) do not improve in precision by IAR.
- *Clock parameters* benefit from IAR only through the position and ZTD parameters. In case the stated parameters are *a priori* known, the clock solutions become uncorrelated with the DD float ambiguities, thus remaining unchanged after ambiguity fixing.
- *Estimable receiver and satellite phase biases* benefit from IAR through the DD float ambiguities, thus always being correlated with them. Due to the presence of their code-driven satellite- and receiver-averaged components, the UD phase biases are less correlated with the DD float ambiguities compared to their SD counterparts.

To further quantify the precision gain of the parameters, we used the concept of *gain numbers* and took a *geometric* approach. The corresponding results are:

- *Slant ionospheric parameters*: While the DD ionospheric solutions experience two orders of magnitude precision improvement, the other-than-DD solutions have quite distinct responses to IAR. Depending on their deviation angle from the DD functions, their standard deviation can improve by factors of 1 to 7 (for the UD components) and 8 to 19 (for the SD components), cf. Fig. 9. The larger the numbers of receivers and satellites, the smaller their deviation angle from the DD functions becomes, thereby more precision gains are experienced by the UD and SD ionospheric solutions (cf. 46).
- *Clock parameters*: Their precision gains do very much depend on the strength of the model's geometry. The weaker the model's geometry, the more the precision gain is experienced by the clock solutions. When the model's geometry is weakest (i.e., geometry-free scenario), the variance of the satellite clock solutions gets smaller by a factor of n (the number of receivers). In this case, the precision gain of the satellite clock solutions increases as the number of network receivers increases (cf. 51).
- *Phase biases*: The between-frequency combined phase biases can have different responses to IAR. For instance, the L1 phase biases very much depend on the strength of the model's geometry. When the model's geometry is strongest (i.e., the geometry-fixed scenario), they hardly benefit from IAR as the corresponding gain number is close to 1. Other combinations such as wide-lane, however, can considerably benefit from IAR *irrespective* of the model's strength (cf. Fig. 12). Similar to the satellite clock solutions, the precision gain of the satellite phase-bias solutions increases as the number of network receivers increases (cf. 66).

Acknowledgements The network processing results in Figs. 4, 6 and 7 were obtained by Curtin PPP-RTK Software, developed at the Curtin GNSS Research Centre. The second author is the recipient of an Australian Research Council (ARC) Federation Fellowship (project number FF0883188). All this support is gratefully acknowledged.

Appendix

In this appendix we denote the variance matrix of a *random matrix*, say X, by $\mathsf{D}(X)$ just for the sake of presentation. It should be interpreted as

$$\mathsf{D}(X) := \mathsf{D}(\mathrm{vec}(X)) \tag{71}$$

Variance matrices of the DD parameters Applying the conditional least-squares adjustment to the DD model (19), the float variance matrices of the DD parameters are shown to read (Khodabandeh and Teunissen 2015)
Float variance matrices:

$$\begin{aligned}\mathsf{D}\left(\hat{\check{t}}^{1S}_{1R}\right) &= \left(\frac{1}{k}c^2_{\check{t}|\rho} + \frac{k-1}{k}c^2_{\check{t}|\rho}\right)\\ &\quad\times\left\{\left(D_n^T C_R D_n\right)\otimes\left(D_m^T C_S D_m\right)\right\}\\ &\quad+\left(\frac{1}{k}\left[c^2_{\check{t}} - c^2_{\check{t}|\rho}\right] + \frac{k-1}{k}\left[c^2_{\check{t}} - c^2_{\check{t}|\rho}\right]\right)\\ &\quad\times\left\{\left(D_n^T C_R D_n\right)\otimes\left(D_m^T C_S \mathcal{P}_{D_{m\rho}} D_m\right)\right\}\end{aligned} \tag{72}$$

$$\begin{aligned}\mathsf{D}\left(\hat{\check{\rho}}^{1S}_{1R}\right) &= \left(\frac{1}{k}c^2_{\check{\rho}} + \frac{k-1}{k}c^2_{\check{\rho}}\right)\\ &\quad\times\left\{\left(D_n^T C_R D_n\right)\otimes\left(D_m^T C_S \mathcal{P}_{D_{m\rho}} D_m\right)\right\}\end{aligned} \tag{73}$$

$$\begin{aligned}\mathsf{D}\left(\hat{\check{a}}^{1S}_{1R}\right) &= \frac{1}{k}\left(D_n^T C_R D_n\right)\otimes\left\{Q_{|\rho}\otimes\left(D_m^T C_S D_m\right)\right.\\ &\quad\left.+(Q - Q_{|\rho})\otimes\left(D_m^T C_S \mathcal{P}_{D_{m\rho}} D_m\right)\right\}\end{aligned} \tag{74}$$

Their fixed counterparts follow by setting $k \to \infty$. This yields
Fixed variance matrices:

$$\begin{aligned}\mathsf{D}\left(\check{\check{t}}^{1S}_{1R}\right) &= c^2_{\check{t}|\rho}\left\{\left(D_n^T C_R D_n\right)\otimes\left(D_m^T C_S D_m\right)\right\}\\ &\quad+\left[c^2_{\check{t}} - c^2_{\check{t}|\rho}\right]\left\{\left(D_n^T C_R D_n\right)\otimes\left(D_m^T C_S \mathcal{P}_{D_{m\rho}} D_m\right)\right\}\end{aligned} \tag{75}$$

$$\mathsf{D}\left(\check{\check{\rho}}^{1S}_{1R}\right) = c^2_{\check{\rho}}\left\{(D_n^T C_R D_n)\otimes\left(D_m^T C_S \mathcal{P}_{D_{m\rho}} D_m\right)\right\} \tag{76}$$

The cofactor matrices Q and $Q_{|\rho}$ are given in Table 2. The projector $\mathcal{P}_{D_{m\rho}}$ is expressed as

$$\mathcal{P}_{D_{m\rho}} = D_{m\rho}\left(D_{m\rho}^T C_S D_{m\rho}\right)^{-1} D_{m\rho}^T C_S \tag{77}$$

where

$$D_{m\rho} = D_m\left(D_m^T C_S D_m\right)^{-1} D_m^T G_1^S \tag{78}$$

Proof of Lemma 1 We use the definition of gain number (25) as

$$\begin{aligned}\gamma(l_{DD}) &= \frac{l_{DD}^T\,\mathsf{D}\left(\hat{\check{\iota}}_R^S\right) l_{DD}}{l_{DD}^T\,\mathsf{D}\left(\check{\check{\iota}}_R^S\right) l_{DD}} \\ &= \frac{\bar{l}^T\,\mathsf{D}\left(\hat{\check{\iota}}_{1R}^{1S}\right)\bar{l}}{\bar{l}^T\,\mathsf{D}\left(\check{\check{\iota}}_{1R}^{1S}\right)\bar{l}}, \qquad \bar{l} = \left(D_n^+ \otimes D_m^+\right) l_{DD}\end{aligned} \tag{79}$$

in which use is made of the identity (38). Substitution of (72) and (75) into the second expression of (79) gives

$$\gamma(l_{DD}) = \frac{\left(\frac{1}{k}c_{\check{\iota}|\rho}^2 + \frac{k-1}{k}c_{\check{\iota}|\rho}^2\right) + \left(\frac{1}{k}\left[c_{\check{\iota}}^2 - c_{\check{\iota}|\rho}^2\right] + \frac{k-1}{k}\left[c_{\check{\iota}}^2 - c_{\check{\iota}|\rho}^2\right]\right)\cos^2(\psi_\iota)}{c_{\check{\iota}|\rho}^2 + \left[c_{\check{\iota}}^2 - c_{\check{\iota}|\rho}^2\right]\cos^2(\psi_\iota)} \tag{80}$$

from which (40) follows. The cosine-squared term of the deviation angle $\psi_\iota = \measuredangle_{l_{D_\rho}}^{l_{DD}}$ follows as

$$\cos^2(\psi_\iota) = \frac{l_{D_\rho}^T\, C\, l_{D_\rho}}{l_{DD}^T\, C\, l_{DD}}, \quad l_{D_\rho} = \mathcal{P}_{D_\rho} l_{DD} \tag{81}$$

where $C = C_R \otimes C_S$. The projector $\mathcal{P}_{D_\rho}$ reads (cf. 77)

$$\mathcal{P}_{D_\rho} = \mathcal{P}_{D_n} \otimes \mathcal{P}_{D_{m\rho}} \tag{82}$$

□

Proof of Lemma 2 Since only the integer ambiguities are assumed to be constant and the remaining parameters are considered unlinked in time, the other-than-DD models (16)–(18) have *no* redundancy. Thus, the number of observations is as many as the number of unknowns. The other-than-DD solutions follow then by inverting the $2f \times 2f$ design matrix

$$\begin{bmatrix} e_f, & -\mu, & \Lambda, & 0 \\ e_f, & +\mu, & 0, & E \end{bmatrix} \tag{83}$$

for each model. Applying the error propagation law to their corresponding mutually uncorrelated ionospheric solutions gives

$$\begin{aligned}&\mathsf{D}\left(e_m\,\hat{\check{\iota}}_{\check{r}}^{\bar{s}}\,e_n^T\right) + \mathsf{D}\left(e_m\,\hat{\check{\iota}}_{1R}^{\bar{s}}\,D_n^+\right) + \mathsf{D}\left(D_m^{+T}\,\hat{\check{\iota}}_{\check{r}}^{1S}\,e_n^T\right) \\ &\quad = c_{\hat{\iota}_2}^2 (C_R \otimes C_S)\mathcal{P}_{DD}^{\perp}\end{aligned} \tag{84}$$

where $\mathcal{P}_{DD}^{\perp} = I - \mathcal{P}_{DD}$. This, together with the canonical decomposition

$$\tilde{\iota}_R^S = \left[e_m,\, D_m^{+T}\right]\begin{bmatrix} \tilde{\iota}_{\check{r}}^{\bar{s}}, & \tilde{\iota}_{1R}^{\bar{s}} \\ \tilde{\iota}_{\check{r}}^{1S}, & \tilde{\iota}_{1R}^{1S} \end{bmatrix}\begin{bmatrix} e_n^T \\ D_n^+ \end{bmatrix}, \tag{85}$$

shows that

$$\mathsf{D}\left(\check{\tilde{\iota}}_R^S\right) = c_{\hat{\iota}_2}^2 (C_R \otimes C_S)\mathcal{P}_{DD}^{\perp} + \mathsf{D}\left(D_m^{+T}\check{\tilde{\iota}}_{1R}^{1S} D_n^+\right) \tag{86}$$

With the role of $\mathcal{A}$ taken by the DD subspace, substitution of (86) into the definition of reduction factor (34) gives

$$r_x = \frac{1+\nu^2}{1+\frac{\nu^2}{\gamma(l_{DD})}}\;;\; \nu^2 = \frac{c_{\hat{\iota}_2}^2}{c_{\check{\iota}|\rho}^2 + \left[c_{\check{\iota}}^2 - c_{\check{\iota}|\rho}^2\right]\cos^2(\psi_\iota)}\tan^2(\theta_\iota) \tag{87}$$

which is equal to (45). The deviation angle $\theta_\iota = \measuredangle_{l_{DD}}^{l}$ follows from the cosine-squared term

$$\cos^2(\theta_\iota) = \frac{l^T\, C\, \mathcal{P}_{DD} l}{l^T\, C\, l}, \quad C = C_R \otimes C_S \tag{88}$$

For the special case $C = I_{mn}$ (i.e., when $C_R = I_n$ and $C_S = I_m$), the DD projector (38) is reduced to

$$\mathcal{P}_{DD} = \left[I_n - \frac{1}{n}e_n e_n^T\right] \otimes \left[I_m - \frac{1}{m}e_m e_m^T\right], \tag{89}$$

proving the equality (46). □

Proof of Lemma 3 With $\Delta\tilde{x}_1 = 0$, an application of the CD-transformation gives

$$-d\tilde{\check{\iota}}^{1S} = \tilde{\rho}_{\check{r}}^{1S} + \tilde{\rho}_{1R}^{1S} D_n^+ u_1 \tag{90}$$

Thus,

$$\begin{aligned}\mathsf{D}(d\hat{\check{\iota}}^{1S}) &= \mathsf{D}\left(\hat{\tilde{\rho}}_{\check{r}}^{1S}\right) + \mathsf{D}\left(\hat{\tilde{\rho}}_{1R}^{1S} D_n^+ u_1\right) \\ \mathsf{D}(d\check{\check{\iota}}^{1S}) &= \mathsf{D}\left(\hat{\tilde{\rho}}_{\check{r}}^{1S}\right) + \mathsf{D}\left(\check{\tilde{\rho}}_{1R}^{1S} D_n^+ u_1\right)\end{aligned} \tag{91}$$

Similar to (84), applying the error propagation law to the non-dispersive solution of (18) results in

$$\mathsf{D}\left(\hat{\tilde{\rho}}_{\check{r}}^{1S}\right) = \frac{c_{\hat{\rho}_2}^2}{n}\left(D_m^T C_S D_m\right) \tag{92}$$

in which the receiver-specific cofactor matrix C_R is assumed to take the special form $C_R = I_n$. The float and fixed variance matrices of the SD satellite clocks are obtained by substituting (92), (73) and (76) into (91). This yields

$$\begin{aligned}\mathsf{D}(d\hat{\tilde{t}}^{1S}) &= \tfrac{c^2_{\hat{\rho}_2}}{n}\left(D_m^T C_S D_m\right) \\ &\quad + \left[\tfrac{1}{k}c^2_{\hat{\rho}} + \tfrac{k-1}{k}c^2_{\check{\rho}}\right]\left[\tfrac{n-1}{n}\right]\left(D_m^T C_S \mathcal{P}_{D_{m\rho}} D_m\right) \\ \mathsf{D}(d\check{\tilde{t}}^{1S}) &= \tfrac{c^2_{\hat{\rho}_2}}{n}\left(D_m^T C_S D_m\right) + c^2_{\check{\rho}}\left[\tfrac{n-1}{n}\right]\left(D_m^T C_S \mathcal{P}_{D_{m\rho}} D_m\right)\end{aligned} \tag{93}$$

The gain number (48) follows then from

$$\begin{aligned}\gamma(l_{D_m}) &= \frac{l_{D_m}^T\, \mathsf{D}(d\hat{\tilde{t}}^S)\, l_{D_m}}{l_{D_m}^T\, \mathsf{D}(d\check{\tilde{t}}^S)\, l_{D_m}} \\ &= \frac{\bar{l}^T\, \mathsf{D}(d\hat{\tilde{t}}^{1S})\, \bar{l}}{\bar{l}^T\, \mathsf{D}(d\check{\tilde{t}}^{1S})\, \bar{l}}, \qquad \bar{l} = D_m^+ l_{D_m}\end{aligned} \tag{94}$$

The cosine-squared term of $\psi_{dt} = \measuredangle_{l_{D_{m\rho}}}^{l_{D_m}}$ is given by (cf. 77)

$$\cos^2(\psi_{dt}) = \frac{l_{D_{m\rho}}^T\, C_S\, l_{D_{m\rho}}}{l_{D_m}^T\, C_S\, l_{D_m}}, \quad l_{D_{m\rho}} = \mathcal{P}_{D_{m\rho}} l_{D_m} \tag{95}$$

□

Proof of Lemma 4 Similar to (92), applying the error propagation law to the non-dispersive solutions of (16)-(17) results in

$$\mathsf{D}\left(e_m\, \tilde{\rho}_{\tilde{r}}^{\bar{s}}\right) + \mathsf{D}\left(e_m\, \tilde{\rho}_{1R}^{\bar{s}}\, D_n^+ u_1\right) = c^2_{\hat{\rho}_2}\, C_S \mathcal{P}^{\perp}_{D_m} \tag{96}$$

with $\mathcal{P}^{\perp}_{D_m} = I - \mathcal{P}_{D_m}$. This, together with (93), gives the float and fixed variance matrices of the satellite clocks through

$$\begin{aligned}\mathsf{D}(d\hat{\tilde{t}}^S) &= \mathsf{D}\left(e_m\, \hat{\tilde{\rho}}_{\tilde{r}}^{\bar{s}}\right) + \mathsf{D}\left(e_m\, \hat{\tilde{\rho}}_{1R}^{\bar{s}}\, D_n^+ u_1\right) + \mathsf{D}\left(D_m^{+T} d\hat{\tilde{t}}^{1S}\right) \\ \mathsf{D}(d\check{\tilde{t}}^S) &= \mathsf{D}(e_m\, \hat{\tilde{\rho}}_{\tilde{r}}^{\bar{s}}) + \mathsf{D}\left(e_m\, \hat{\tilde{\rho}}_{1R}^{\bar{s}}\, D_n^+ u_1\right) + \mathsf{D}\left(D_m^{+T} d\check{\tilde{t}}^{1S}\right)\end{aligned} \tag{97}$$

With the role of $\mathcal{A}$ taken by the SD subspace D_m, substitution of $\mathsf{D}(d\check{\tilde{t}}^S)$ into the definition of reduction factor (34) gives

$$r_x = \frac{1+\nu^2}{1+\frac{\nu^2}{\gamma(l_{D_m})}}\,; \quad \nu^2 = \frac{c^2_{\hat{\rho}_2}}{\frac{1}{n}c^2_{\hat{\rho}_2} + \left[\frac{n-1}{n}\right]c^2_{\check{\rho}}\cos^2(\psi_{dt})}\tan^2(\theta_{dt}) \tag{98}$$

which is equal to (55). The deviation angle $\theta_{dt} = \measuredangle_{l_{D_m}}^{l}$ follows from the cosine-squared term

$$\cos^2(\theta_{dt}) = \frac{l^T\, C_S\, \mathcal{P}_{D_m} l}{l^T\, C_S\, l} \tag{99}$$

For the special case $C_S = I_m$, the SD projector (37) is reduced to

$$\mathcal{P}_{D_m} = I_m - \frac{1}{m} e_m e_m^T, \tag{100}$$

proving the equality (56). □

Proof of Lemma 5 Given the decomposition ($\Delta\tilde{x}_1 = 0$)

$$d\tilde{t}_{1R} = \tilde{\rho}_{1R}^{\bar{s}} - G_1^{\bar{s}} \Delta\tilde{x}_{1R}, \tag{101}$$

the proof goes along the same lines as that of Lemma 3. The deviation angle $\psi_g = \measuredangle_{g}^{e_m^{+T}}$ follows from the cosine-squared term

$$\cos^2(\psi_g) = \frac{e_m^+\, C_S\, \mathcal{P}_G\, e_m^{+T}}{e_m^+\, C_S\, e_m^{+T}}, \quad \mathcal{P}_G = C_S^{-1} G_1^S \left(G_1^{S^T} C_S^{-1} G_1^S\right)^{-1} G_1^{S^T} \tag{102}$$

□

Proof of Lemma 6 The proof goes along the same lines as those of Lemmas (1) –(5). □

References

Baarda W (1973) S-transformations and criterion matrices. Tech. rep., Netherlands Geodetic Commission, Publ. on Geodesy, New Series, vol 5(1), Delft

Banville S (2016) GLONASS ionosphere-free ambiguity resolution for precise point positioning. J Geod 90(5):487–496

Collins P, Bisnath S, Lahaye F, Heroux P (2010) Undifferenced GPS ambiguity resolution using the decoupled clock model and ambiguity datum fixing. Navigation 57(2):123–135

Coster AJ, Gaposchkin EM, Thornton LE (1992) Real-time ionospheric monitoring system using the GPS. Navigation 39(2):191–204

de Jonge PJ (1998) A processing strategy for the application of the GPS in networks. Ph.D. thesis, Delft University of Technology, Publication on Geodesy, 46, Netherlands Geodetic Commission, Delft

Delporte J, Mercier F, Laurichesse D, Galy O (2007) Fixing integer ambiguities for GPS carrier phase time transfer. In: Frequency control symposium, 2007 joint with the 21st European frequency and time forum. IEEE International, IEEE, pp 927–932

Fliegel H, Beard R, Landis G, Stebbins S (1990) An alternative common view method for time transfer with GPS. Navigation 37(3):263–272

Ge M, Gendt G, Rothacher M, Shi C, Liu J (2008) Resolution of GPS carrier-phase ambiguities in precise point positioning (PPP) with daily observations. J Geod 82(7):389–399

Geng J, Shi C, Ge M, Dodson AH, Lou Y, Zhao Q, Liu J (2012) Improving the estimation of fractional-cycle biases for ambiguity resolution in precise point positioning. J Geod 86(8):579–589

Giorgi G, Teunissen PJG, Gourlay TP (2012) Instantaneous global navigation satellite system (GNSS)-based attitude determination for maritime applications. IEEE J Ocean Eng 37(3):348–362

Gunther C, Henkel P (2012) Integer ambiguity estimation for satellite navigation. IEEE Trans Signal Process 60(7):3387–3393

Han S (1997) Quality-control issues relating to instantaneous ambiguity resolution for real-time GPS kinematic positioning. J Geod 71(6):351–361

Hassibi A, Boyd S (1998) Integer parameter estimation in linear models with applications to GPS. IEEE Trans Signal Process 46(11):2938–2952

Hauschild A, Grillmayer G, Montenbruck O, Markgraf M, Vörsmann P (2008) GPS based attitude determination for the flying laptop satellite. Springer, Netherlands, pp 211–220

Henderson HV, Pukelsheim F, Searle SR (1983) On the history of the kronecker product. Linear Multilinear Algebra 14(2):113–120

Jonkman N, Teunissen P, Joosten P, Odijk D (2000) GNSS long baseline ambiguity resolution: impact of a third navigation frequency. In: Geodesy Beyond 2000, IAG Symp 121, pp 349–354

Khodabandeh A, Teunissen PJG (2015) An analytical study of PPP-RTK corrections: precision, correlation and user-impact. J Geod 89(11):1109–1132

Khodabandeh A, Teunissen PJG (2016) Array-aided multifrequency GNSS ionospheric sensing: estimability and precision analysis. IEEE Trans Geosci Remote Sens 54(10):5895–5913

Laurichesse D, Mercier F, Berthias J, Broca P, Cerri L, CNES F (2009) Integer ambiguity resolution on undifferenced GPS phase measurements and its application to PPP and satellite precise orbit determination. Navigation 56(2):135–149

Li B, Verhagen S, Teunissen PJG (2014) Robustness of GNSS integer ambiguity resolution in the presence of atmospheric biases. GPS Solut 18(2):283–296

Liao X, Gao Y (2001) High-precision ionospheric TEC recovery using a regional-area GPS network. Navigation 48(2):101–111

Nadarajah N, Teunissen PJG, Raziq N (2013) Instantaneous GPS-Galileo attitude determination: single-frequency performance in satellite-deprived environments. IEEE Trans Veh Technol 62(7):2963–2976

Odijk D, Zhang B, Khodabandeh A, Odolinski R, Teunissen PJG (2015) On the estimability of parameters in undifferenced, uncombined GNSS network and PPP-RTK user models by means of S-system theory. J Geod 90(1):15–44

Odolinski R, Teunissen PJG (2017) Low-cost, high-precision, single-frequency GPS-BDS RTK positioning. GPS Solut. https://doi.org/10.1007/s10291-017-0613-x

Petit G, Jiang Z, Uhrich P, Taris F (2000) Differential calibration of Ashtech Z12-T receivers for accurate time comparisons. In: Proceedings of 14th European frequency and time forum (Turin), pp 40–44

Plumb J, Larson KM, White J, Powers E (2005) Absolute calibration of a geodetic time transfer system. IEEE Trans Ultrason Ferroelectr Freq Control 52(11):1904–1911

Schaer S (1999) Mapping and predicting the Earths ionosphere using the global positioning system. Ph.D. thesis, University of Bern, Bern, Switzerland

Schaer S, Beutler G, Mervart L, Rothacher M, Wild U (1995) Global and regional ionosphere models using the GPS double difference phase observable. In: Proceedings of the IGS workshop on special topics on new directions, 77-92 Potsdam, Germany, May 15–27

Teunissen PJG (1985) Generalized inverses, adjustment, the datum problem and S-transformations. In: Grafarend EW, Sanso F (eds) Optimization and design of geodetic networks. Springer, Berlin

Teunissen PJG, Joosten P, Tiberius CCJM (1999) Geometry-free ambiguity success rates in case of partial fixing. In: Proceedings of ION-NTM, pp 25–27

Teunissen PJG, Khodabandeh A (2014) Do GNSS parameters always benefit from integer ambiguity resolution? A PPP-RTK network scenario. In: Proceedings of ION GNSS+, Tampa, Florida, pp 590–600

Teunissen PJG (1995) The least-squares ambiguity decorrelation adjustment: a method for fast GPS integer ambiguity estimation. J Geod 70(1–2):65–82

Teunissen PJG (1997) A canonical theory for short GPS baselines. Part I: the baseline precision. J Geod 71(6):320–336

Teunissen PJG, Kleusberg A (1998) GPS for geodesy, 2nd edn. Springer, Berlin

Teunissen PJG, de Jonge PJ, Tiberius CCJM (1997) Performance of the LAMBDA method for fast GPS ambiguity resolution. Navigation 44(3):373–383

Teunissen PJG, Odijk D, Zhang B (2010) PPP-RTK: results of CORS network-based PPP with integer ambiguity resolution. J Aeronaut Astronaut Aviat 42(4):223–229

Tiberius CCJM, de Jonge PJ (1995) Fast positioning using the LAMBDA method. In: Proceedings of the 4th international symposium on differential satellite navigation systems, Bergen, Norway, 24–28 April, Citeseer, vol 30

Xu P, Shi C, Liu J (2012) Integer estimation methods for GPS ambiguity resolution: an applications oriented review and improvement. Survey Rev 44(324):59–71

Zhang B, Teunissen PJG (2015) Characterization of multi-GNSS between-receiver differential code biases using zero and short baselines. Sci Bull 60(21):1840–1849

Zhang B, Teunissen PJG, Yuan Y (2017) On the short-term temporal variations of GNSS receiver differential phase biases. J Geod 91(5):563–572